SEMMELWEIS EGYETEM

DOKTORI ISKOLA

Ph.D. értekezések

3264.

CZOCH ÁKOS

Celluláris és molekuláris élettan

című program

Programvezető: Dr. Hunyady László, egyetemi tanár

Témavezető: Dr. Rácz Frigyes Sámuel, egyetemi adjunktus

INVESTIGATING CORRELATIONS OF RESTING-STATE FRACTAL BRAIN CONNECTIVITY AND COGNITIVE PERFORMANCE IN HEALTHY AGING

PhD thesis

Czoch Ákos, PharmD

Semmelweis University Doctoral College

Molecular Medicine Division

Supervisor: Frigyes Sámuel Rácz, MD, PhD

Official reviewers: Levente Herényi, PhD

László Négyessy, D.Sc

Head of the Complex Examination Committee:

László Smeller, D.Sc

Members of the Complex Examination Committee:

Éva Ruisanchez, MD, PhD

Csaba Karabélyos, PharmD, PhD

Budapest

2025

Table of Contents

List of Abbreviations

BFMF: bivariate focus-based multifractal formalism

BL: Baseline

CANTAB: Cambridge Neuropsychological Test Automated Battery

CGSA: Coarse-Graining Spectral Analysis

DCCA: Detrended Cross-Correlation Analysis

DMS: Delayed Matching to Sample

ECoG: Electrooculography

ECT: Electroconvulsive therapy

EEG: Electroencephalography

FC: Functional connectivity

FDR: False Discovery Rate Method

FrC: Fractal connectivity

HE: Healthy elderly

HFD: Higuchi's Fractal Dimension

HY: Healthy young

ICA: Independent Component Analysis

IRASA: Irregular Resampling Auto-Spectral Analysis

MARA: Multiple Artefact Rejection Algorithm

MOT: Motor Screening Task

MRCSA: Multiple-Resampling Cross-Spectrum Analysis

PAL: Paired Associates Learning

PALFAM28: Paired Associates Learning First Attempt Memory score

PALTA: Paired Associates Learning Total Attempts

PRM: Pattern Recognition Memory

RTI: Reaction Time

RVP: Rapid Visual Information Processing

RVPA: Rapid Visual Information Processing sensitivity

RVPPH: Rapid Visual Information Processing precise identifying of sequences

SWM: Spatial Working Memory

SWMBE12: Spatial Working Memory Between Errors for 12 boxes

SWMBE468: Spatial Working Memory Between Errors for 4,6,8 boxes

SWMTE12: Spatial Working Memory Total Errors for 12 boxes

SWMTE468: Spatial Working Memory Total Errors for 4,6,8 boxes

WG: Word generation

Symbols

$\bar{S}_{XX_h}$: corrected fractal power spectrum

$\bar{S}_h(\omega)$: fractal power spectrum (as denoted in IRASA)

$\overline{SS}_h(\omega)$: fractal cross-power spectrum at frequency ω

S_{XX_h}: fractal power spectrum (as denoted in CGSA)

$SF_{XY}(\omega)$: fractal cross-power spectrum for all frequencies

$SH_{XY}(\omega)$: oscillatory cross-power spectrum for all frequencies

$SS_{xy}(\omega)$: cross-spectral power at frequency ω

S_{XX}: auto-power spectrum

$\overline{Y(\omega)}$: complex conjugate of $Y(\omega)$

r_s: sampling rate

$\alpha_x(\omega)$/ $\beta_x(\omega)$: phase of the wave at frequency ω

c: constant

f: frequency

$f_x(t)$: fractal signal

h: resampling factor

H: Univariate Hurst-exponent

h^H: rescaling factor

$h_x(t)$: oscillatory signal

H_{xy}: bivariate hurst-exponent

$K^2{}_{xy}$: squared spectrum coherency

β: Univariate spectral slope

β_{xy}: bivariate spectral slope

ω: angular frequency

$F(\omega)$ / $Y(\omega)$= Fourier transform at angular frequency ω

ω: angular frequency

1 Introduction

1.1 The Complexity and Functional Connectivity of the Human Brain

The human brain is an extraordinary organ, renowned for its complexity and capability. Encompassing several billion neurons, the brain facilitates an extensive range of functions that are essential for survival and interaction with the environment. These functions include basic physiological processes such as breathing and heart rate regulation, as well as more advanced activities like perception, language, memory, and reasoning. The architecture of the brain is intricately organized into distinct regions, each dedicated to specific roles. For instance, the occipital lobe is primarily involved in visual processing (1), the temporal lobe in auditory perception and memory (2), and the frontal lobe in executive functions and decision-making (3, 4). Despite their specialized roles, these regions do not function in isolation. Instead, they engage in constant communication, forming a highly integrated network that enables the brain to execute complex functions and tasks. Consequently, evaluating the functional connectivity (FC) of the brain – i.e., how the distinct brain regions interact with one another (5) – has gained significant traction through the past decades. The aim of this notion was to achieve a better understanding of the system-level neurophysiological foundation of mental processes and functioning (6). Earlier research has described that specific groups of brain regions form functional networks through their synchronized activity, including the default mode network (7), the task positive network (8), and the dorsal and frontotemporal attention networks (9). One particular relevance – among others – of such research lies in that it helps understanding alterations in cognitive functions related to aging from a multitude of aspects.

1.2 Alterations of Connectivity in Healthy Aging

1.2.1 Cognitive Decline

It is well known that even in healthy aging several physiological functions gradually start to deteriorate, including the cardiovascular, respiratory, skeletomuscular or immune systems (10-12). Furthermore, the decline in cognitive abilities during healthy aging (13, 14), in the absence of any pathological condition (15, 16), is particularly significant. The effects of aging-related cognitive decline are various and far-reaching. It affects a plethora

of daily activities decreasing quality of life and also carries physiological and socio-economical consequences (17). Additionally, even with the methods and tools of current biomedical technology it is a strenuous and difficult task to distinguish naturally occurring loss of cognitive capacity from early dementia or developing Mild Cognitive Impairment (18). In these conditions early diagnosis is essential for an effective intervention, thus it is an especially important issue. Consequently, numerous studies aimed to find neurophysiological markers connected to various aspects of healthy aging; however, only a handful of biomarkers have been discovered that can be resolutely linked to loss of cognitive capabilities (19).

1.2.2 Functional Network Topology

It has been established in preceding studies that the aging brain demonstrates distinct functional network topology compared to those of younger individuals (20-22). As of now, the extent and precise nature of such changes are not fully understood; however, it is speculated that the cell and subsequent function loss, plus the resulting compensatory mechanisms manifest in these alterations (23, 24). Additionally, connections have been uncovered between resting-state FC patterns and performance in cognitive tests in the elderly population (25-27). FC has been proved to be affected in several clinical conditions (28) – predominantly in older individuals – that has an impact on cognitive functioning, for instance Alzheimer's Disease, Parkinson's Disease (29) or Mild Cognitive Impairment. Moreover, the severity of the symptoms was associated with connectivity measures (30-32). Considering another angle, earlier studies – employing a wide variety of imaging modalities – found that functional networks go through a reorganization reacting to the amplified mental workload or during task solving (33-37). The explanation behind this phenomenon might be that throughout task completion - in order to be more efficient - unnecessary connections should be trimmed and the appropriate ones for the task at hand activated (38). Also, it was suggested that such a task-related reorganization could be differing in the aged population compared to the youth. This notion is supported by recent evidence demonstrating age-related differences in task-induced functional reorganization, particularly within theta oscillatory networks. Gómez-Lombardi et al. (2024) (39) revealed that older adults exhibit slower individual frontal theta frequencies and weaker effective connectivity during an auditory inhibitory control task compared to younger adults. These alterations were associated with

diminished task performance, suggesting that the reduced capacity for efficient network reorganization of the aging brain may reflect underlying changes in oscillatory dynamics and connectivity patterns. This phenomenon in the elderly brain is possibly the manifestation of the diminished ability to handle increased workload (40). A 2024 review by Tanaka et al. (41) highlighted the potential of electroencephalography-based (EEG) markers for early detection of cognitive decline in older adults. They found that increased theta/alpha brain wave ratio and alterations in FC patterns may indicate early cognitive changes, even before a structural shift in the brain is apparent. Based on these considerations, FC might offer valuable insight into cognitive changes associated with aging and their underlying neurophysiological mechanisms. Nevertheless, despite these recent efforts markers that might link brain connectivity pattern changes to age-related alterations in cognition are scarce, and therefore more research is warranted in this direction (24, 42-46).

1.3 Fractal Dynamics in Complex Systems and Brain Networks

Many complex systems express fractal dynamics manifesting as long-term autocorrelations decaying according to a power-law function. Such processes are often of natural phenomena (47), geophysical systems (48, 49), meteorological data (50), financial markets (51, 52) or functional brain networks (53-55). These systems share a common property: their statistical properties exhibit power-law scaling. Moreover, scale-free (or fractal) correlations are expressed both within the univariate dynamics of their separate components and within their interactions, too. In the former scenario, the autocorrelation function of the process demonstrates slow decay, whereas in the latter, a similar pattern is observed in the cross-correlation function of the two assessed processes. Regardless, a fundamental aspect of both situations is the ability to establish a power-law relationship between the correlation and the scale of observation (56). The same holds true in the frequency domain, as well. In that case, long-range coupling is indicated by the power-law dependency of auto- and cross-spectral power on the frequency (57). Commonly, the attained fractal scaling exponent is used to characterize this power-law relationship, termed the Hurst exponent (H) in the time- and spectral slope (β) in the frequency domain. The two measures are related and inherently equivalent (57, 58). In the case of brain activity, fractal dynamics most commonly denotes the long-term autocorrelation in univariate neural fluctuations (58, 59). However, the importance of identifying long-term

couplings of distinct brain regions – and thus extending fractal analysis to the connectivity domain – lies in the fact that it can provide insight on the functional organization of the brain in a way which single-scale or scale dependent analyses cannot. For this reason, recent years saw an upsurge in research interest towards fractal connectivity (FrC) (53, 54, 60-62). Novel research has further expanded the application of fractal measures to clinical contexts, offering unique insights into neurophysiological changes associated with therapeutic interventions. For instance, Denier et al. (2024) (63) utilized Higuchi's Fractal Dimension (HFD) – a measure of temporal complexity – to assess neuroplasticity induced by electroconvulsive therapy (ECT) in patients with depression. Their study demonstrated significant increases in HFD values within the anterior and posterior hippocampi following ECT, indicating enhanced complexity and irregularity in neural activity. These results align with prior evidence linking fractal scaling properties to cognitive performance and underscore the utility of fractal analysis for exploring brain dynamics beyond traditional connectivity measures.

1.3.1 The Fractal Nature of Neural Activity and Functional Connectivity

As stressed previously, it has been established by earlier studies that neural activity displays fractal temporal scaling in its dynamics, and this property can be characterized with a scaling exponent both in the time and frequency domains (64). Despite the fact that the exact neural foundation of this scale-free nature is not yet completely understood, its physiological relevance is indicated by previous evidence showing that the fractal scaling exponent varies in various scenarios, such as during sustained attention (51), in certain psychiatric conditions like schizophrenia (65) or in aging (66-68). Recent research by Seeburger et al. (69) further supports this notion, demonstrating that time-varying functional connectivity of low-frequency fluctuations across different brain networks varies with fluctuations in sustained attention. These findings align with and extend the work of Achard and colleagues (53) who demonstrated that this phenomenon is not exclusively present in regional (i.e., univariate) neural activity, but it manifests in the coordinated activity across different brain regions, too. As a matter of fact, several studies – employing a wide selection of imaging modalities and techniques – confirmed since then the fractal scaling nature of FC dynamics (60, 70-72). Moreover, in a recent study FrC patterns were also found altered in reaction to a pattern recognition test, meant to induce increased mental workload (62), implying that FrC and cognitive functioning are

connected. Generally, one can apply two approaches in FrC assessment: i) connectivity is estimated in a time-resolved manner and then the fractal scaling is determined from the fluctuations in the acquired measurements (73-76), or ii) the power-law or scale-free coupling is computed directly and the fractal nature of the data is described through the bivariate scaling exponent (56, 57, 61, 77). Several techniques have been devised for both strategies; however, a common limitation of them is that in order to produce unbiased results the input data needs to be a purely fractal signal, devoid of any harmonic or oscillatory components. Thus, it is important to evaluate the degree of bias these components introduce in the estimation of fractal measures, not only for the characterization of the bias itself, but mainly because the two constituents (fractal and oscillatory) of the signal might also capture/represent separate underlying mechanisms. This concept in the case of neural activity is of key importance, as neurophysiological fluctuations are known as a combination of broad- and narrow-band (i.e. fractal and oscillatory) activities in an EEG recording: oscillatory components appear at characteristic frequencies such as theta or alpha oscillations, superimposed on a scale-free "background" activity (64, 78, 79). Additionally, the mechanisms producing these fluctuations are presumed to be exceedingly dissimilar in the two instances (80, 81). The same concept is also relevant in the context of brain functional connectivity. For example, synchronized alpha activity could manifest as a peak overlaid on the otherwise broadband cross-coherence spectrum (82). Therefore, isolating the fractal constituents from the rest of the signal seems to be crucial in assessing fractal attributes of neural activity, and this holds true for both univariate and multivariate scenarios.

1.3.2 Fractal Analysis of Neural Activity

For univariate fractal analysis of electrocorticography (ECoG) recordings, He and colleagues (78) employed a method called coarse-graining spectral analysis (CGSA) in order to prune the power-spectra of the signals from oscillatory spikes and thus counteract the bias they introduce in the estimation of the spectral slope. The method was first proposed by Yamamoto and Hughson (83) whom later developed it further (84). Originally, they employed this approach in hear-rate variability analyses and interestingly, the method was applied to trim the fractal components from the data, not the oscillatory. In summary, CGSA takes advantage of the self-affine characteristics of fractal processes; more precisely, when the process is resampled at a different time scale,

the statistical distribution of the data remains unchanged (85). What this means is that the power spectrum of a fractal process remains the same only adjusted by the resampling factor and Hurst exponent after resampling, whereas in an oscillatory signal the spikes get relocated by the change in sampling rate (for more details, see **section 3.1.1**). To put it differently, for a given frequency this means that after resampling, power will remain as non-zero if the process displays fractal characteristics, while it will drop to nearly zero if the signal is only periodic at that frequency. This phenomenon enables one to recreate the power spectrum of a fractal signal by calculating the cross-spectrum of the original signal and its resampled version (83, 84). Building upon the same principles, Wen and Liu (86) introduced a more advanced method called irregular resampling auto-spectral analysis (IRASA) to differentiate between fractal and oscillatory components in neural activity. IRASA addresses several limitations of CGSA – such as its incapacity to manage numerous oscillatory components that are interconnected through the scaling factor – by using a series of non-integer rescaling factors, instead of only two. Specifically, additional details are available in the Methods section.

Despite their many advantages, neither CGSA or IRASA can be employed in bivariate signal analysis, only in univariate scenarios (i.e. individual recordings). Additionally, identical difficulties arise when one is to explore FC in the frequency domain. The broadband cross-coherency spectrum, which implies fractal connectivity, might contain oscillatory peaks – the manifestation of e.g. extensive cortical alpha synchronization – even in resting (82) or during mental exercise (87). Therefore, methods that can remove the effects of such scale-dependent interactions and set apart the scale-free constituent of statistical interdependence are essential for a deeper understanding of fractal brain connectivity. For this reason, our lab started to develop an extension of the IRASA method to the bivariate case, which we later termed Multiple-Resampling Cross-Spectral analysis (MRCSA) for separating the fractal constituent within the cross-spectral density of paired neurophysiological signals (88). MRCSA can provide a theoretically unbiased estimate of the fractal cross-spectrum and consequently the cross-spectral slope, and while its ability to completely isolate the oscillatory constituents is hindered by the potentially intricate interactions between fractal and oscillatory components, it can contribute valuable insights into fractal connectivity by evaluating the ratio of fractal to overall cross-spectral power. Furthermore, MRCSA enables unbiased assessment of

fractal properties, not just in regional neural activity but also in fractal connectivity networks.

In summary, functional connectivity and fractal dynamics of neurophysiological signals appear as a hallmark for complex brain functioning, which warrants further research. Specifically, these traits appear to be relevant for cognitive functions, as well as they were found altered in healthy aging, in line with reduced cognitive capabilities. Therefore, we hypothesized that integrating the two concepts of fractal dynamics and functional connectivity within *fractal connectivity* analysis could offer novel and useful neural markers connecting age-related alterations in brain network topology to decline in cognitive abilities. I was intrigued and captivated by the concept of fractal connectivity and its plausible physiological relevance and implications, and thus I made it the primary subject of interest during my PhD studies. My overall goal was to apply this concept on physiological data to explore conditions where it might prove to be valuable according to previous research. In what follows, I will demonstrate that fractal connectivity indeed plays a relevant role in adapting to increased mental workload, as well as I will show how it is affected in healthy aging and related changes in cognitive capabilities.

2 Objectives

Fractal connectivity is an emerging concept in neuroscience that fuses the theory of functional connectivity with the well-known scale-free characteristic of neural dynamics; however, its physiological relevance is not yet understood. Accordingly, my work had two main objectives. My first goal was to validate our recently developed MRCSA technique to assess fractal connectivity in in vivo EEG recordings. Since both functional brain connectivity and fractal dynamics of regional neural activity had been previously associated with increased mental workload, I hypothesized that performing a simple cognitive task (such as word generation) would result in a reorganization of fractal connectivity networks. Then, my second goal was to utilize this method to better understand how fractal connectivity might reflect changes in neural dynamics related to healthy aging, and how these patterns might explain lower cognitive performance commonly observed in elderly individuals, even in the absence of a pathological condition. In line, both reduced functional connectivity and reduction of long-term correlations were previously reported in aging, and these changes were often found associated with cognitive performance in various tasks. Therefore, I hypothesized that fractal connectivity could be a sensitive tool to assess both aspects simultaneously. Finally, to better understand how these neural patterns relate to cognition, I intended to contrast them with performance measures from a wide range of cognitive tasks indicative in age-related cognitive decline.

3 Materials and Methods

This section is organized as follows.

- First, I briefly summarize the core characteristics of fractal time series and show how this property can be exploited to separate the fractal component of a process from other (e.g., oscillatory) signal constituents, as well as how and why this method can be particularly relevant in the analysis of neural recordings. Then, I demonstrate how this technique can be generalized to multivariate time series to analyse fractal connectivity, yielding our MRCSA method.
- Second, I describe the dataset and the performed analyses that were utilized to validate MRCSA dataset on EEG recordings collected in resting-state and while performing a simple word generation task.
- Finally, I introduce the study we performed to investigate how fractal connectivity patterns change in healthy aging and how these neural signatures relate to cognitive performance in the young and elderly.

3.1 Fractal processes and connectivity

3.1.1 Self-affinity of fractal processes

To demonstrate the self-affine property, let us have a fractal process $f\ (t)$ and resample it with $h\ >\ 0$ resampling factor where the resampled version is $f_h(t) = f(t/h)$. The process is 'up-sampled' when $h\ >\ 1$ and 'down-sampled' if $0 < h < 1$. For instance, in the case of $h = 2$ $f_h(t)$ is equal to $f(t)$ sampled at double the original rate, whereas $h = 1/2$ means that $f_h(t)$ only contains every second sample from $f(t)$. Importantly, in case of a fractal process the statistical distribution of the signal remains unchanged, and the characteristic self-affinity of fractal processes can be described as

$$f_h(t) \triangleq\ h^H f(t)\ , \tag{1}$$

where H is the Hurst exponent (58). This equation means that resampling $f(t)$ by h results in the same distribution as previously, only rescaled by factor h^H in the resampled $f_h(t)$ time series (59, 84, 85). Additionally, subjecting $f(t)$ and $f_h(t)$ to the Fourier transformation, this self-affine property can be equivalently recognized as the frequency-scaling attribute:

$$F_h(\omega) \triangleq h^H F(\omega)\,, \tag{2}$$

where $F(\omega)$ and $F_h(\omega)$ correspond to the amplitudes of $f(t)$ and $f_h(t)$ at angular frequency ω. The angular frequency ω and sampling rate r_s relate to each other as $\omega = 2\pi r_s$. Relatedly, fractal processes show a continuous, broadband frequency distribution. Within such a distribution, the relationship between spectral power (i.e. the squared amplitude) and frequency is described by a power-law function with a scaling exponent β_x. Furthermore, in most cases spectral power shows an inverse proportionality to frequency (59). One can formalise these concepts as

$$|F(\omega)|^2 \propto c \times \omega^{-\beta}\,, \tag{3}$$

where c is a constant. Consequently, the spectral power of a fractal signal is non-zero all through the spectrum and if illustrated on a log-log scale, it adheres to a straight line (linear function) with a slope being $-\beta_x$. It must be emphasised that β_x and H are related and essentially the same as they capture identical scaling characteristics of the process (58, 85). In summary, power or amplitude spectrum is statistically similar after resampling, except for being rescaled by factor h^H in case of a fractal process. In contrast, the power spectrum of a periodic/oscillatory signal $x(t)$ containing a distinct set of sinusoidal elements with its characteristic frequencies ω_i will be zero (or nearly zero) everywhere except where the specific characteristic frequencies correspond to the constituting sinusoids. Particularly, resampling a periodic signal results in the non-zero 'peaks' relocating in the power spectrum, conforming to h, while the spectral power remains zero elsewhere, even including the original characteristic frequencies. **Figure 1**. illustrates the above-mentioned effects of resampling. Taking advantage of this peculiarity offers solutions when one means to separate or decompose the power spectrum

of a signal of mixed nature (containing periodic/oscillatory and fractal signals as well) into fractal and oscillatory components.

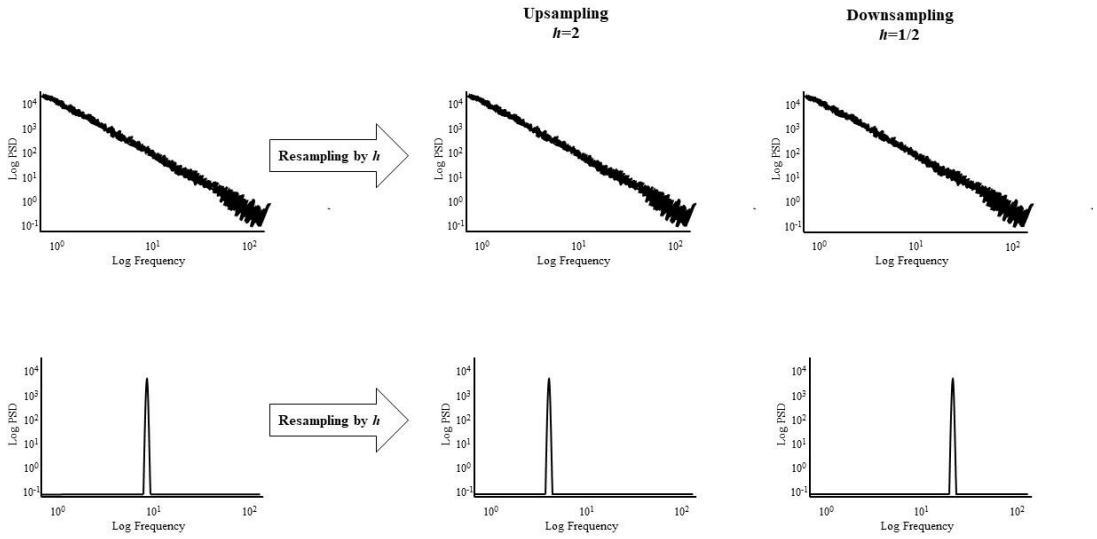

Figure 1.*The effects of resampling. The upper panel showcases the power spectrum of a purely fractal signal and its up- and downsampled versions. The lower panel illustrates the power spectrum of a purely oscillatory signal and that of its resampled versions. The power spectrum of the fractal signal remains unchanged (in distribution) while in the latter case the oscillatory peak gets relocated according to the resampling factor h.*

3.1.2 Separating the fractal component of the power spectrum

3.1.2.1 Coarse Graining Spectral Analysis (CGSA)

Yamamoto and Hughson (83) were the first to introduce a method called Coarse Graining Spectral Analysis (CGSA) not to separate the fractal component of a broadband spectrum, but to reduce the fractal 'background' noise. Their team studied heart rate variability time series thus they used this approach to eliminate the fractal component granting a better estimation of the oscillatory peaks, the focal point of their work. In their study, firstly, the cross-spectral power was computed from the original signal X and the 'coarse-grained' (i.e. resampled by $h = 2^{-1}$) and rescaled (by dividing it by h^{-H}) version X_h, obtaining the fractal power spectrum S_{XX_h}. Then, to procure the oscillatory component, the authors simply subtracted the fractal elements from the auto-power spectrum of the original signal S_{XX} (83). However, an inherent limitation of the method is that H needs to be estimated

beforehand (see below). Expanding on the previously mentioned concepts, the authors took advantage of (i) resampling and rescaling a fractal process should yield an equivalent amplitude spectrum as the original. Consequently, their cross-spectrum will be non-zero throughout all frequencies. However, in contrast, (ii) the cross-spectrum of a periodic signal and its resampled variant will gravitate to zero across all frequencies, thanks to the shift of the non-zero amplitudes in the spectra.

Despite the highly perceptive nature of this approach, it had a number of shortcomings. First of those being the need to estimate H prior to CGSA. For this purpose, the authors used rescaled range analysis (89). This issue was soon resolved by resampling by two different factors, h and its reciprocal $1/h$ (84). This method yielded two versions, one rescaled by h^H and one by $1/h^H = h^{-H}$. Then, taking the two cross-spectra denoted as S_{XX_h} and $S_{XX_{1/h}}$ and their geometric mean as

$$\bar{S}_{XX_h} = \sqrt{\left\|S_{XX_h}\right\| \cdot \left\|S_{XX_{1/h}}\right\|}, \tag{4}$$

where $\bar{S}_{XX_h}$denotes the corrected fractal power spectrum, then the separate estimation of H is no longer needed. Also worth noting the independence of this method from the rescaling factor $h > 0$. However, there is a more serious limitation of CGSA as per Wen and Liu (86), namely that there are non-negligible interactions between the fractal and oscillatory constituents of a signal, thus the cross-spectrum of the original and the resampled version of a process containing both will have the same issue preventing the total elimination of periodic peaks. Lastly, when numerous oscillatory peaks are present and the characteristic frequencies relate to each other as $\omega_i = h \times \omega_j$ or $\omega_i = 1/h \times \omega_j$, it inhibits the workings of CGSA. As a result, the CGSA technique needed to be developed further to ameliorate these limitations.

3.1.2.2 Irregular-Resampling Auto-Spectral Analysis (IRASA)

Accordingly, Wen and Liu (86) proposed Irregular Resampling Auto-Spectral Analysis (IRASA) – a method building on the foundations of CGSA – as a way to overcome the aforementioned obstacles. In such a simple model the process $y(t)$ is comprised of a fractal $f(t)$ and an oscillatory $x(t)$ constituent:

$$y(t) = f(t) + x(t). \tag{5}$$

The method makes the assumption that the examined signal $y(t)$ is completely without additive noise. In accordance with the linearity property, if one applies the Fourier transform to $y(t)$ it yields

$$Y\ (\omega) = F(\omega)e^{-j\alpha_x(\omega)} + X(\omega)e^{-j\beta_x(\omega)}, \tag{6}$$

where the amplitude and the phase of the fractal constituent at frequency ω is indicated by $F(\omega)$ and $\alpha_x(\omega)$, respectively, and for the oscillatory constituent $X(\omega)$ and $\beta_x(\omega)$ denote the same terms. Next, if one resamples $y(t)$ by factors h and $1/h$ ($h > 0$) and marks the new versions as $y_h(t)$ and $y_{1/h}(t)$, then the auto-spectral power at a given ω frequency, with similar notation as in Eq. (6), can be described as

$$\begin{aligned} S_{y_h y_h}(\omega) = {} & \left[F_h(\omega)e^{-j\alpha_h(\omega)} + X_h(\omega)e^{-j\beta_h(\omega)}\right]\left[F_h(\omega)e^{j\alpha_h(\omega)}\right. \\ & \left. + X_h(\omega)e^{j\beta_h(\omega)}\right] \end{aligned} \tag{7}$$

for $y(t)$, and for $y_{1/h}(t)$

$$\begin{aligned} S_{y_{1/h}y_{1/h}}(\omega) = {} & \left[F_{1/h}(\omega)e^{-j\alpha_{1/h}(\omega)} + \right. \\ & \left. X_{1/h}(\omega)e^{-j\beta_{1/h}(\omega)}\right]\left[F_{1/h}(\omega)e^{j\alpha_{1/h}(\omega)} + X_{1/h}(\omega)e^{j\beta_{1/h}(\omega)}\right]. \end{aligned} \tag{8}$$

Consequently, by utilizing the concept outlined in Eq. (2), the above listed equations (7) and (8) can be rearranged as

$$S_{y_h y_h}(\omega) = h^{2H}F^2(\omega)\left\|1 + \frac{X_h(\omega)}{F_h(\omega)}e^{j\alpha_h(\omega) - j\beta_h(\omega)}\right\|^2 \tag{9}$$

and

$$S_{y_{1/h}y_{1/h}}(\omega) = h^{-2H}F^2(\omega)\left\|1 + \frac{X_{1/h}(\omega)}{F_{1/h}(\omega)}e^{j\alpha_{1/h}(\omega) - j\beta_{1/h}(\omega)}\right\|^2. \tag{10}$$

Then, taking the geometric mean of the two auto-spectra similarly to Eq. (4) the initial estimation of the fractal power spectrum $\bar{S}_h(\omega)$ becomes possible, independently of h and H as

$$\bar{S}_h(\omega) = \sqrt{S_{y_h y_h}(\omega) S_{y_{1/h} y_{1/h}}(\omega)} =$$

$$= F^2(\omega) \left\| 1 + \frac{X_h(\omega)}{F_h(\omega)} e^{j\alpha_h(\omega) - j\beta_h(\omega)} \right\| \left\| 1 + \frac{X_{1/h}(\omega)}{F_{1/h}(\omega)} e^{j\alpha_{1/h}(\omega) - j\beta_{1/h}(\omega)} \right\|. \quad (11)$$

If one considers an oscillatory constituent $x(t)$ which is comprised only of a single sinusoid at harmonic frequency ω_0, then, according to Eq. (11) $\bar{S}_h(\omega) \neq F^2(\omega)$ solely in two instances:

a) $\bar{S}_h(\omega) = F^2(\omega) \left\| 1 + \frac{X_h(\omega)}{F_h(\omega)} e^{j\alpha_h(\omega) - j\beta_h(\omega)} \right\|$ if $\omega = h\omega_0$ and (12)

b) $\bar{S}_h(\omega) = F^2(\omega) \left\| 1 + \frac{X_{1/h}(\omega)}{F_{1/h}(\omega)} e^{j\alpha_{1/h}(\omega) - j\beta_{1/h}(\omega)} \right\|$ if $\omega = \omega_0/h$.

In these cases, the estimation of the fractal spectrum is dependent on h and thus $\bar{S}_h(\omega)$ produces biased results, meaning that the oscillatory component is not completely eliminated, only attenuated. However, utilizing a series of different resampling factors the oscillatory power at ω_0, which is non-zero at this point, is relocated to a different frequency at each instance. Exploiting this during the estimation process in using distinct resampling factors and their reciprocals, one gets a set of fractal power estimates for all frequencies. These yields will centralize to the true $F^2(\omega)$ save for the cases of Eq. (12), where usually one outlier corresponds to h. Accordingly, taking the median of these estimates at the separate frequencies will result in an unbiased estimate of $F^2(\omega)$ for all ω, insofar as the amount of the outliers does not exceed 50% of the number of estimates (86). Importantly, IRASA becomes robust against the occurrence of several oscillatory components if one employs a large enough set of h and $1/h$ factor pairs through decreasing the chance of them being related as $\omega_i = h \times \omega_j$ or $\omega_i = 1/h \times \omega_j$.

Finally, the power spectrum of a mixed signal as in Eq. (5) is obtained as

$$Y^2(\omega) = Y(\omega)\overline{Y(\omega)} = F^2(\omega) + X^2(\omega) + 2F(\omega)X(\omega)\cos\big(\alpha(\omega) - \beta(\omega)\big) \quad (13)$$

where $\overline{Y(\omega)}$ is the complex conjugate of $Y(\omega)$. Note, that the mixed power spectrum is comprised of fractal and oscillatory spectral densities and an additional confounding term. Importantly, the confounding term is defined by the phase difference of the fractal and

oscillatory elements. However, assuming the two elements are uncoupled, the second part of the confounding term is expected to be zero thus the whole confounding term can be eliminated by utilizing numerous sections of data and averaging it over the acquired spectra (86). Keep in mind, that this also assumes that the process is stationary during the sections employed. Finally, the theoretically unbiased estimate of the oscillatory power spectrum can be obtained by subtracting the fractal power spectrum from the original/mixed spectrum (86). With the assistance of IRASA, the fractal spectral exponent can be determined from only the fractal component, without the distorting effects of oscillatory constituents, which is particularly important in the case of neural signals which are known for their composite nature (i.e. broadband activity and alpha peaks)

3.1.3 Extension to fractal connectivity: Multiple-Resampling Cross-Spectral Analysis

Despite IRASA improving upon many shortcomings of CGSA, the method is still only applicable in univariate scenarios, while long-term correlations could very well be found between multiple as cross-correlation (52, 90, 91). Detrended cross-correlation analysis (DCCA) by Podobnik and Stanley (56) was the first-proposed method to assess such long-range fractal coupling between two non-stationary processes. This technique quickly gained traction and was soon extended to the multifractal domain (92). Additionally, numerous other time-domain methods expanded on it including the detrended moving-average cross-correlation analysis (93) and the height cross-correlation analysis (77). Yet, all of these methods have the same limitation: they are susceptible to the bias introduced by the presence of oscillatory components (see below). Fractal scaling in the bivariate case is analogous to the univariate one in that it is characterized by a scaling exponent. For processes x and y the bivariate fractal scaling or bivariate Hurst exponent is denoted as H_{xy}(77). Furthermore, Kristoufek (57) proved that the analogy between the Hurst exponent and spectral scaling exponent holds true in the bivariate case, too, i.e., long-range fractal coupling can be assessed also in the frequency domain and characterized with the cross-spectral scaling exponent. Specifically, in the event of long-term fractal interaction or coupling among processes x and y the relationship between cross-spectral power and frequency is established through a power-law function:

$$\left|SS_{xy}\right|(\omega) \propto c \times \omega^{-\beta_{xy}}, \tag{14}$$

where $SS_{xy}(\omega)$ denotes the cross-spectral power, ω as the frequency and the cross-spectral exponent as β_{xy}.

This equation is analogous to Eq. (3) - and is the foundation to Multiple-Resampling Cross-Spectral Analysis - only in the bivariate case and β_{xy} and H_{xy} are similarly correspondent as β_x and H_x (57, 94). MRCSA is the extension of IRASA to the bivariate domain, so that the bivariate fractal exponent can be estimated without the distorting effects of oscillatory components. Additionally, this scaling property manifests in the frequency domain, as well. If one takes two processes of fractal nature $k(t)$ and $l(t)$ with a bivariate Hurst exponent H_{kl}, then using h as resampling factor on the processes, their new cross-spectrum $SS_{k_h l_h}(\omega)$ will be identical to the original cross-spectrum $SS_{kl}(\omega)$ rescaled by $h^{H_{kl}}$ as

$$\left|SS_{k_h l_h}(\omega)\right| \triangleq h^{H_{kl}} |SS_{kl}(\omega)|. \tag{15}$$

One may demonstrate it through applying the form in Eq. (13) to gain the cross-spectrum:

$$\begin{aligned} SS_{k_h l_h}(\omega) &= F_{k_h}(\omega)\overline{F_{l_h}(\omega)} = h^{H_k} F_k(\omega)\overline{h^{H_l} F_l(\omega)} \\ &= h^{H_k + H_l} F_k(\omega)\overline{F_l(\omega)} = h^{2H_{kl}} SS_{kl}(\omega). \end{aligned} \tag{16}$$

Eq. (15) and (16) shows that $H_{xy} = \frac{H_x + H_y}{2}$, which has been derived theoretically in antecedent studies (56, 95-97). More specifically, from the three possible scenarios only two are feasible:

- $H_{xy} = \frac{H_x + H_y}{2} \Rightarrow 2\left(H_x + H_y - 2H_{xy}\right) = 0 \Rightarrow \lim_{\omega \to 0+} K_{xy}^2(\omega) \propto const. \Rightarrow$ ✓
- $H_{xy} < \frac{H_x + H_y}{2} \Rightarrow 2\left(H_x + H_y - 2H_{xy}\right) > 0 \Rightarrow \lim_{\omega \to 0+} K_{xy}^2(\omega) = 0 \Rightarrow$ ✓
- $H_{xy} > \frac{H_x + H_y}{2} \Rightarrow 2\left(H_x + H_y - 2H_{xy}\right) < 0 \Rightarrow \lim_{\omega \to 0+} K_{xy}^2(\omega) = +\infty \Rightarrow$ ✗ ,

where $K_{xy}^2(\omega)$ is the squared spectrum coherency at frequency ω. As $K_{xy}^2(\omega)$ lies between 0 and 1, the last case contradicts these boundaries, thus it is infeasible. (96, 98, 99) (99). Consequently, following the notions described in Eq. (7)-(12) and exploiting

this property, one could construct a method to extract the fractal element from the cross-spectrum. This technique, which we termed Multiple Resampling Cross-Spectral Analysis (defined as MRCSA previously) is the direct extension of IRASA from the univariate to the bivariate domain, and its main purpose is to provide unbiased estimates of the cross-power spectral exponent. **Figure 2.** illustrates the main steps of MRCSA.

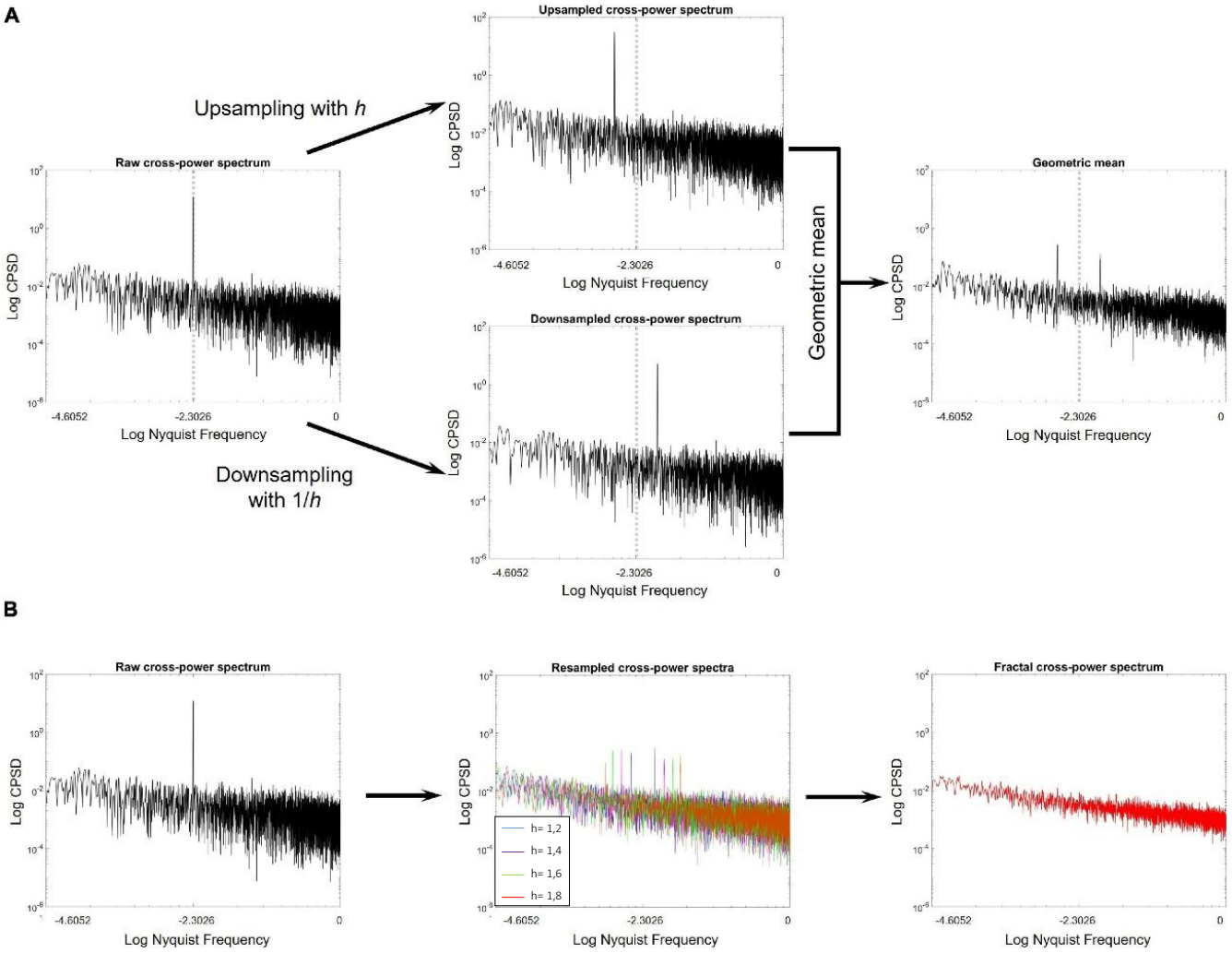

Figure 2. *Main steps of the MRCSA procedure.* ***A****: The left panel displays the cross-power spectrum acquired from a pair of long-range cross-correlated time series with a highly correlated oscillatory constituent at 10 Hz. The middle panels present the cross-power spectra after the signals have been upsampled (top) and downsampled (bottom) by factors* h *and* $1/h$*, respectively. It is evident that resampling shifts the oscillatory peak from its 'original position' at 10 Hz in both instances. The right panel illustrates the geometric mean of the up- and downsampled corss-spectra.* ***B****: The left panel shows the raw cross-spectrum. The middle panel displays the geometric means of the upsampled and*

downsampled cross-spectra after resampling with different values of h. Lastly, by taking the median, one can acquire the fractal cross-power spectrum, lacking an oscillatory peak (88).

More elaborately, if one takes two processes of mixed nature, $x(t) = f_x(t) + h_x(t)$ and $y(t) = f_y(t) + h_y(t)$ with Hurst exponents of H_x and H_y, respectively, where $f_x(t)$ is the fractal and $h_x(t)$ is the oscillatory or harmonic component (not to be confused with h, the rescaling factor), then one can gain the cross-spectrum of $x(t)$ and $y(t)$, denoted as $\left|SS_{xy}(\omega)\right|$:

$$\left|SS_{xy}(\omega)\right| = \left|F_x(\omega)\overline{F_y(\omega)}\right|, \tag{17}$$

where the Fourier transforms of $x(t)$ and $y(t)$ are denoted as $F_x(\omega)$ and $F_y(\omega)$. Following the resampling procedure with h and $1/h$, we get four different time series: $x_h(t)$, $y_h(t)$, $x_{1/h}(t)$ and $y_{1/h}(t)$. Let us define the Fourier transforms of the fractal components as $FX_h(\omega)e^{-j\alpha_h(\omega)}$ and $FY_h(\omega)e^{-j\gamma_h(\omega)}$ and of the oscillatory or harmonic components as $HX_h(\omega)e^{-j\beta_h(\omega)}$ and $HY_h(\omega)e^{-j\delta_h(\omega)}$, in the case of series $x_h(t)$ and $y_h(t)$. For $x_{1/h}(t)$ and $y_{1/h}(t)$ the notation is analogous with what has been described previously. From here, the cross-power spectrum of $x_h(t)$ and $y_h(t)$ can be acquired as

$$\begin{aligned} SS_{x_h y_h}(\omega) = \left[FX_h(\omega)e^{-j\alpha_h(\omega)} + HX_h(\omega)e^{-j\beta_h(\omega)}\right] \\ \left[FY_h(\omega)e^{j\gamma_h(\omega)} + HY_h(\omega)e^{j\delta_h(\omega)}\right] = \\ = h^{H_x+H_y}FX(\omega)FY(\omega)e^{-j(\alpha_h(\omega)-\gamma_h(\omega))} \\ \left(1 + \frac{HX_h(\omega)}{FX_h(\omega)}e^{-j(\alpha_h(\omega)-\beta_h(\omega))}\right)\left(1 + \frac{HY_h(\omega)}{FY_h(\omega)}e^{j(\gamma_h(\omega)-\delta_h(\omega))}\right) \end{aligned} \tag{18}$$

and in an equivalent manner for $x_{1/h}(t)$ and $y_{1/h}(t)$:

$$\begin{aligned} SS_{x_{1/h} y_{1/h}}(\omega) = \left[FX_{1/h}(\omega)e^{-j\alpha_{1/h}(\omega)} + HX_{1/h}(\omega)e^{-j\beta_{1/h}(\omega)}\right] \\ \left[FY_{1/h}(\omega)e^{j\gamma_{1/h}(\omega)} + HY_{1/h}(\omega)e^{j\delta_{1/h}(\omega)}\right] = \end{aligned} \tag{19}$$

$$= h^{-(H_x+H_y)} FX(\omega)FY(\omega)e^{-j(\alpha_{1/h}(\omega)-\gamma_{1/h}(\omega))}$$

$$\left(1+\frac{HX_{1/h}(\omega)}{FX_{1/h}(\omega)}e^{-j(\alpha_{1/h}(\omega)-\beta_{1/h}(\omega))}\right)\left(1+\frac{HY_{1/h}(\omega)}{FY_{1/h}(\omega)}e^{j(\gamma_{1/h}(\omega)-\delta_{1/h}(\omega))}\right).$$

Then, the fractal cross-power spectrum, connoted as $\overline{SS}_h(\omega)$, can be estimated by taking the geometric mean of $\left\|S_{x_h y_h}(\omega)\right\|$ and $S_{x_{1/h} y_{1/h}}$:

$$\begin{aligned}\overline{SS}_h(\omega) &= \sqrt{\left\|S_{x_h y_h}(\omega)\right\| \left\|S_{x_{1/h} y_{1/h}}(\omega)\right\|} \\ &= |FX(\omega)FY(\omega)|\sqrt{\|1+A_h(\omega)\|\|1+B_h(\omega)\|\left\|1+C_{1/h}(\omega)\right\|\left\|1+D_{1/h}(\omega)\right\|},\end{aligned} \tag{20}$$

where

- $A_h(\omega) = \frac{HX_h(\omega)}{FX_h(\omega)} e^{-j(\alpha_h(\omega)-\beta_h(\omega))}$
- $B_h(\omega) = \frac{HY_h(\omega)}{FY_h(\omega)} e^{j(\gamma_h(\omega)-\delta_h(\omega))}$
- $C_{1/h}(\omega) = \frac{HX_{1/h}(\omega)}{FX_{1/h}(\omega)} e^{-j(\alpha_{1/h}(\omega)-\beta_{1/h}(\omega))}$ and
- $D_{1/h}(\omega) = \frac{HY_{1/h}(\omega)}{FY_{1/h}(\omega)} e^{j\left(\gamma_{1/h}(\omega)-\delta_{1/h}(\omega)\right)}$.

These terms describe the relationship of the fractal and oscillatory elements in regard of their ratio of magnitudes and phase differences. Note that these terms and Eq. (20) let us draw similar conclusions as with IRASA, specifically:

i. If $x(t)$ and $y(t)$ are composed solely of fractal elements then $\overline{SS}_h(\omega)$ equals to the fractal cross-power spectrum and since all confounding terms are rendered zero at all ω, the estimation is unbiased.

ii. In the event of $x(t)$ containing a harmonic element with characteristic frequency denoted as ω_{HX}, the term $A_h(\omega)$ will exhibit a non-zero value at $\omega_1 = h\omega_{HX}$ and similarly term $C_{1/h}(\omega)$ will be non-zero at $\omega_2 = h/\omega_{HX}$. As a result, the estimated spectral slope of $\overline{SS}_h(\omega)$ is biased at ω_1 and ω_2.

iii. If $y(t)$ contains a harmonic element with characteristic frequency denoted as ω_{HY}, the term $B_h(\omega)$ will exhibit a non-zero value at $\omega_3 = h\omega_{HY}$ and similarly term

$D_{1/h}(\omega)$ will be non-zero at $\omega_4 = h/\omega_{HY}$. As a result $\overline{SS}_h(\omega)$ is biased at ω_3 and ω_4.

Importantly, the cases of ii. and iii., when the fractal cross-power spectrum cannot be estimated without bias, are dependent on the rescaling factor h. Calculating $\overline{SS}_h(\omega)$ with a variety of different h values (analogously with IRASA), the frequencies at which the estimation error manifest will be different for each h. Using a set of $\overline{SS}_h(\omega)$ estimates, all with disparate h values, and taking the median for each h across all ω frequencies, one can obtain the unbiased estimate of the fractal cross-power spectrum. However, if the amount of outliers (number of the occurring estimation errors) exceed 50% of the number of estimates at the given frequency, the final estimate is no longer unbiased (86, 100). With that, we derive the formula for unbiased estimation of the fractal cross-power spectrum for all ω, denoted $SF_{XY}(\omega)$:

$$SF_{XY}(\omega) = median_h\{\overline{SS}_h(\omega)\}, \tag{21}$$

Finally, one may strive for an unbiased estimate of the oscillatory cross-power spectrum $SH_{XY}(\omega)$. It is found that computing $|SS_{XY}(\omega)|^2$ similarly to Eq. (13) involves not only $SF_{XY}(\omega)$, $SH_{XY}(\omega)$ and the confounding terms based on relative phase differences, but also interaction terms between fractal and oscillatory elements of $x(t)$ and $y(t)$. While averaging cross-power spectra from several data segments helps eliminate confounding terms assuming no coupling between components, interaction terms remain unaffected by phase differences and cannot be excluded by averaging. Thus, while MRCSA offers an unbiased estimate strictly of the fractal cross-power spectrum, it does not ensure unbiased estimation of the oscillatory cross-power spectrum. Nonetheless, a maximum ceiling to the participation of the oscillatory elements in the cross-power spectrum can be determined by taking the percentage of fractal cross-power to the mixed (full) cross-spectral power:

$$\%Fractal = \frac{\sum_\omega SF_{XY}(\omega)}{\sum_\omega SS_{XY}(\omega)} \times 100, \tag{22}$$

for all frequencies ω.

There are two essential notions to discuss further. First, if one takes Eq. (17)-(21) and makes $x(t) = y(t)$, the method returns the simple, univariate IRASA formula. Second, if one calculates the fractal and oscillatory spectra of $x(t)$ and $y(t)$ separately with IRASA and their fractal cross-power spectrum with MRCSA, the confounding interaction terms of $|SS_{XY}(\omega)|^2$ can be ousted thus theoretically an unbiased estimate of oscillatory cross-spectral power can be gained. However, the scope of our team was to construct a method to estimate fractal cross-spectral power thus this will not be considered here any further.

3.1.3.1 The Multiple Resampling Cross-Spectral Analysis algorithm

To preserve coherence between the uni- and bivariate cases, the MRCSA algorithm follows the same blueprint as introduced by Wen and Liu (86) for IRASA.

i. Fifteen segments, which overlap partially, are picked from a given pair of signals. All segments cover 90% of the original datasets and have equal number of time stamps. The difference between the starting time indices is kept constant and thus the segments are evenly spaced.

ii. First, the mixed cross-power spectrum $SS_{xy}(\omega)$ is estimated for the first segment in accordance with Eq. (17). Using fast Fourier transforming and Hanning windowing, one attains the Fourier transforms. The frequency resolution is established at twice the smallest power of 2 that surpasses the number of data points within the time segments. This adjustment is accomplished by zero-padding the time series when needed. The aim is to ensure that if h is less than 2, the amount of frequencies exceed the number of data points in the original signal and its resampled versions, as well.

iii. Using cubic spline interpolation, the segments are resampled by h and $1/h$. In order to avoid aliasing when downsampling, the segments are treated with a low-pass, fast Fourier transform-based filter. The cut-off frequency is set as the sampling rate divided by twice the smallest integer that exceeds the largest h-value. Identically to IRASA, the values of h are set by default between 1.1 and 1.9 using increments of 0.05 yielding 17 different pairs of resampling factors.

iv. For the up- and down-sampled signal pairs the cross-power spectra are attained in a similar manner as detailed in step ii. Note, that the frequency resolution for

both the up- and down-sampled versions (with befitting zero-padding) are the same as for the mixed cross-power spectrum.

v. Next, the geometric mean of the cross-power spectra is calculated for all pairs of $\{h|1/h\}$. Then, for all frequencies the median of the cross-power spectra over all h is used to obtain the unbiased estimate of the fractal cross-power spectrum $SF_{XY}(\omega)$.

vi. Steps ii-v are iterated for each data segments attained in step i, followed by calculating the average of the mixed cross-power spectrum $SS_{xy}(\omega)$ and the fractal cross-power spectrum $SF_{xy}(\omega)$ by computing the arithmetic mean over the cross-spectra acquired from the 15 data segments.

Following the completion of the MRCSA algorithm, one can continue with computing the cross-spectral slope, β_{xy} or the ratio of fractal to mixed cross-spectral power. On a log-log transformed fractal cross-power spectrum the spectral slope can be obtained by ordinary least squares linear regression. However, a straightforward log-log transformation would results in the over-representation of higher frequencies (86), thus after the log transformation the frequency elements are resampled to acquire an even frequency resolution in the log scale. Next, fitting a linear function on the resampled, log-transformed fractal cross-power spectrum by ordinary least squares estimation yields the unbiased spectral slope estimate β_{xy} as the first coefficient of the function. Importantly, the fractal spectral slope is essentially negative (the distribution of cross-spectral power follows $1/\omega^{-\beta_{xy}}$). However, by convention the univariate β_x values are given with reversed signs (59), meaning a steeper cross-spectrum is described with a larger β_x value and the same stands true for the bivariate β_{xy} values. To calculate the fractal cross-spectral power's percentage one may simply apply Eq. (22) in the desired frequency range.

Analogously to IRASA, MRCSA can also be employed in a sliding-window fashion to determine a time-frequency representation of fractal cross-spectral power between two interconnected processes over an extended period.

3.2 Validating Multiple Resampling Cross-Spectral Analysis: Fractal connectivity during increased mental workload

As an initial step before analysing physiological data, we evaluated the MRCSA method in *in silico* experiments. These results are detailed in our original publication Racz et al. (88) in pages 8-12. Briefly, MRCSA was able to estimate the cross-spectral exponent accurately, even in the presence of noise. Precisely, the estimation error was within 5% even at a low signal-to-noise ratio of 10. After this technical validation, my goal was to assess the utility of MRCSA on empirical, *in vivo* signals. For this, I analysed a publicly available EEG dataset (101), as detailed below.

3.2.1 Participants of the in vivo validation

The dataset analysed in this study was made publicly available by Shin and colleagues (101). The entire repository consists of EEG recordings of 26 young, healthy participants (aged 26.1±3.5 years, all right-handed, 17 females and 9 males) collected under varying task conditions, from which we selected the baseline (BL) vs. word generation (WG) paradigm (Dataset C) as it represents a simple case of increased cognitive workload. The original experiment was conducted in line with the Declaration of Helsinki, approved by the institutional review board of the Berlin Institute of Technology (approval number: SH_01_20150330) and all participants provided written informed consent. None of the study subjects reported any history of a neuropsychiatric condition nor was on medication that might affect brain function or cognition. More details on the study population are reported in the original article and supplementary information at Shin et al. (101).

3.2.2 Measurement protocol and data acquisition

In the WG condition, participants were presented a letter at the beginning of each trial, and their task was to come up with as many different words as possible that start with the given letter in 10 seconds. In contrast, during the BL trials participants were instructed to rest for an equal duration and keep their sight on a fixation cross presented in the center of the screen. WG and BL trials were randomized in order and interspersed with inter-trial intervals of about 20 seconds. One recording session consisted of 10 BL and 10 WG trials, and every participant completed three sessions resulting in a total number of 30-30 trials for WG and BL.

During the protocol, EEG data was collected with a 28-channel BrainAmp amplifier (Brain Products GmbH, Gilching, Germany) at a sampling rate of 1000 Hz (down-sampled to 200 Hz before data publication). The monitored cortical regions were standard positions of the international 10-5 system (102) and included Fp1, Fp2, AFF5h, AFF6h, AFz, F1, F2, FC1, FC2, FC5, FC6, Cz, C3, C4, T7, T8, CP1, CP2, CP5, CP6, Pz, P3, P4, P7, P8, POz, O1, and O2 with reference and ground electrodes placed at TP9 and TP10, respectively.

3.2.3 Data pre-processing and analysis

EEG data was pre-processed using the EEGLAB toolbox (103) combined with custom MATLAB functions and scripts. First the data was divided into epochs of 30 seconds, starting at 5 seconds before trial onset and ending at 15 seconds after trial offset, thus consisting of 5 seconds of resting-state/preparation in the beginning, 10 seconds of WG or BL and another 15 seconds of resting-state at the end. This segmentation was required for the automated artefact elimination step (see below) that requires data segments that are at least 16 seconds long. Then, EEG epochs were band-pass filtered with a 4^{th} order zero-phase Butterworth filter with cut-off frequencies 0.5 and 80 Hz, with additional line noise removal at 50 Hz using the *cleanline* algorithm of EEGLAB. Artefacts related to eye movements, blinks, skeletal muscle activity or other extra-neural sources (e.g., heart, white noise) were identified and eliminated using the independent component analysis (ICA)-based multiple artefact rejection algorithm (MARA) (104, 105). Finally, data was re-referenced to the common average electrode, and active 10-second segments of WG and BL were isolated for further analysis (30-30 epochs for WG and BL, 28-channels each, for every subject).

Fractal connectivity analysis was performed using MRCSA. The analysis range was set to 1-25 Hz, and we used the standard set of resampling factors h ranging from 1.1 to 1.9 in increments of 0.05 as recommended by Wen and Liu (86). We investigated two output measures, i) the cross-spectral exponent β_{xy} and ii) the percentage of fractal spectral power in total (mixed) spectral power. These measures were obtained for every channel pair, yielding 28-by-28 matrices for each trial, and then for each subject the 30-30 matrices for both conditions were averaged, yielding statistically robust estimates of the fractal connectivity patterns in WG and BL.

The outcome measures were compared between WG and BL along four axes:

i. The auto-spectral slopes (β_x, IRASA analysis) were compared in a channel-to-channel manner using paired t-tests or Wilcoxon signed rank tests depending on data normality (assessed by Lilliefors test).
ii. The sum of cross-spectral exponents β_{xy} for each channel were contrasted using the same statistical principles. Note that this measure is resemblant of the 'node degree' commonly used in functional connectivity analyses (106).
iii. Cross-spectral exponents were also compared in a connection-to-connection manner.
iv. Percentage of fractal power was also contrasted between WG and BL in a node degree and connection-to-connection fashion.

The level of significance was defined as $p<0.05$, and for each level i.-iv. the outcomes were adjusted for multiple comparisons using the Bonferroni method.

3.3 Investigating fractal connectivity and cognition in healthy aging

After successfully validating MRCSA both *in silico* and *in vivo*, we applied this method in our follow up publication Czoch et al. (107), of which I am the first author. In this study, we investigated fractal connectivity in healthy aging using MRCSA, and addressed its plausible relationships with cognitive performance. Our study involved two cohorts: a healthy young (HY) group, defined as aged between 18-35 years and a healthy elderly (HE) group consisting of individuals over the age of 60 years. In both groups, we only enrolled healthy participants, i.e., those without any documented neuropsychiatric or general medical condition (including medication) that might affect central nervous system or cognition in particular. The study had two key aspects: resting-state neural activity as recorded by EEG, and cognitive performance as assessed by a comprehensive, automated test battery consisting of tasks indicative in age-related cognitive decline or early dementia. Study details are presented in the following.

3.3.1 Participants of the comparative study

A group of 47 volunteers, consisting of 25 young adults (18-35 years old, with a mean age of 25.7 and 12 females) and 22 elderly individuals (over 60 years old, with a mean age of 66.2 and 8 females), participated in this research. The study was conducted in

accordance with the Declaration of Helsinki and received approval from the Semmelweis University Regional and Institutional Committee of Science and Research Ethics (approval no. 2020/6). Prior to the measurement, written informed consent was obtained from all participants. Volunteers were instructed to abstain from substances that might affect cognitive function (e.g., caffeine) for at least 3 hours prior to measurement and have at least 6 hours of sleep the previous night. Individuals who had neuropsychological or psychiatric illnesses, a history of brain damage, were on medication that affects the central nervous system or severe cardiovascular pathologies were excluded from the study. Pregnancy was also an exclusion criterion. All individuals successfully completed the measurement protocol; however, one young and three elderly participants had to be later excluded from further analysis due to excessive head movement and/or inadequate signal quality. Consequently, the final sample size included 24 young (age: 25.37 ± 3.20 years) and 19 elderly (age: 66.39 ± 6.09 years) participants, totalling to 43 participants.

3.3.2 Measurement protocol

The EEG recordings were conducted in the Department of Physiology at Semmelweis University, in a quiet, dimly lit room. The participants sat in a comfortable chair and faced a 24-inch computer screen, which was approximately at 0.8-meter distance throughout the measurement. They were instructed to avoid any movements or facial expressions to reduce signal artefacts. The measurement and ensuing analysis protocol were created and executed using MATLAB. (Mathworks, Natick, MA, United States). The session commenced with a 3-minute eyes-closed resting-state interval, succeeded by an eyes-open resting-state period of equal duration. Please be aware that following the initial recording session, three distinct cognitive paradigms (visual pattern recognition, n-back, maze paradigm) were undertaken for about an hour. Nevertheless, in the present study, our analyses were confined to the EEG data obtained during the eyes-closed resting-state only.

3.3.3 Data acquisition and pre-processing

The EEG data were captured using a wireless Emotive Epoc+ device along with the associated EmotivPRO software (Emotiv Systems Inc., San Francisco, CA, United States). The initiation of data collection began only after maximal contact quality was affirmed, as indicated by the EmotivPRO software (i.e., electrode impedances were kept

under 5 kOhm). The device featured an internal sampling rate of 2048 Hz, with an effective bandwidth between 0.2 to 45 Hz. This is facilitated through the use of a 5th order Sinc filter, with additional notch filters at 50 and 60 Hz. After internally down-sampling the raw data to 256 Hz, it was sent wirelessly to a desktop computer. With the device set up, we could monitor neural activity of 14 brain regions, according to 10-10 standard montage locations, including AF3, AF4, F3, F4, F7, F8, FC5, FC6, T7, T8, P7, P8, O1, and O2. Reference and ground electrodes were positioned at P3 and P4, employing CMS and DRL.

After the application of a further 4th order, zero-phase Butterworth-filter with cut-off frequencies of 0.5 and 45 Hz, the EEG recordings were visually assessed, and epochs uninterrupted by artefacts were selected by two separate investigators for the next stage of analysis. Only those segments that were found to be artefact-free by both investigators independently were included in further analyses. The final epoch length was defined as 72 seconds, being the longest available interval from all recordings. For 4 participants (1 young, 3 elderly) no such segment could be identified, thus we had to exclude them from further processing. Then, the adjusted segments underwent Independent Component Analysis (ICA), for which we used the EEGLAB toolbox (103). Artefacts related to eye movements, skeletal muscle activity or other sources of noise were discerned and eliminated by manually scrutinizing the independent components. Note that the previously utilized, automated MARA tool could not be employed here, as its reliability in terms of artefact detection drops substantially for a low channel number of 14 (104, 105). Independent components associated with artefactual signal constituents were identified based on the characteristics as utilized by MARA, outlined in the work of Gabard-Durnam and colleagues (108). After removing artefact components, we performed reverse ICA, and finally, the data was re-referenced to the common-average electrode.

3.3.4 Cognitive testing: Cambridge Neuropsychological Test Automated Battery (CANTAB)

After concluding the EEG recording session, a baseline assessment of cognitive performance was conducted using seven cognitive tests from the *Cambridge Neuropsychological Test Automated Battery* (CANTAB). CANTAB, initially created by

the University of Cambridge, functions as a precise, standardized and validated assessment tool for various facets of cognition. CANTAB tests include tasks involving working, visual, and spatial memory, as well as learning and executive function, reaction time, information processing, and numerous other cognitive domains, among others. Additionally, they offer insights into the conditions under which a specific test could be the most suggestive. From the range of options, we have chosen seven activities linked to the decline in cognitive function related to ageing and dementia, as outlined by Csipo et al (109). These included the Motor Screening Task (**MOT**), Delayed Match to Sample (**DMS**), Paired Associates Learning (**PAL**), immediate and delayed Pattern Recognition Memory (**PRM**), Reaction Time (**RTI**), Rapid Visual Processing (**RVP**), and Spatial Working Memory (**SWM**) tasks. **Table 1** provides a short description of each task, while for more detailed explanations and video demonstrations the reader is referred to the official CANTAB website (https://www.cambridgecognition.com/cantab/).

Table 1. *Employed **cognitive tests**. **MOT**: Motor Screening Task; **DMS**: Delayed Matching to Sample; **PAL**: Paired Associates Learning; **PRM**: Pattern Recognition Memory; **RTI**: Reaction Time; **RVP**: Rapid Visual Information Processing; SWM: Spatial Working Memory* (modified after Czoch et al. (107))

Name	Description (time in minutes)	Assessed functions	Outcome
MOT	Colored crosses appear on random locations on the screen and the participant must tap on them as fast as possible. (**2**)	Sensorimotor skills	Reaction time, precision
DMS	The participant must choose from 4 visual patterns the one presented before a brief delay (0, 4 or 12 seconds) (**7**)	Short-term visual recognition memory and matching ability	Response latency, number of correct choices
PAL	Boxes are shown on the screen, one or more contains a visual pattern. After opening every box, the patterns are presented one by one and the participant must choose which box they came from. (**8**)	Visual memory and learning	Number of errors and attempts, First attempt memory score
PRM	A series of visually intricate, verbally indescribable patterns are shown to the participant. First, they view two patterns, one familiar and one new, selecting the previously seen pattern. The task is repeated after a 20-minute delay. (**4** and **4**)	Visual pattern recognition memory	Number and percentage of correct responses, response latency
RTI	The participant must hold down a button at the bottom of the screen. One or five buttons are presented on the top of the screen, after a random delay one of them turns yellow and the participant must release the starting- and tap the new button as quickly as possible. (**3**)	Motor- and mental response accuracy, latency and speed	Reaction time, movement time, number of errors
RVP	A series of digits ranging from 2 to 9 are shown in a pseudorandom sequence (100 digits/minute). The participant must identify a specific target sequence (e.g., 3-5-7) and respond by quickly tapping a button. Difficulty increases when participants are required to watch for multiple target sequences simultaneously. (**7**)	Sustained attention	Response latency, correct responses, probability of false alarms, sensitivity
SWM	The participant must search for a token in boxes presented on the screen. After selecting one box, it closes again, and remains on the screen. The difficulty depends on the number of boxes (4, 6, 8 or 12 boxes).(**4**)	Working memory, strategy in problem solving, manipulation of visuospatial information	Between errors, within errors, total errors, strategy

Each task within the battery started with an instructional introduction session, customizable to the user's native language (either Hungarian or English in this study). Participants were required to complete the training before proceeding to the actual test, ensuring a solid grasp of the forthcoming task. To reduce the likelihood of any influence or bias from investigators, participants undertook the CANTAB assessment in isolation within a separate room, which typically lasted 40 to 50 minutes. Subjects engaged in the CANTAB session using a 10.2" iPad tablet computer, for which the tasks were standardized.

3.3.5 Estimating fractal connectivity with Multiple Resampling Cross-Spectral Analysis

In this study, the activity of the brain in resting state was recorded by EEG, a method considered to be non-stationary on longer time scales (110). Accordingly, the previously selected, pre-processed, 72-second-long segments were cut into non-overlapping epochs of 8 seconds, resulting in 9 epochs for each participant. These shorter epochs provided the grounds for fractal connectivity analysis, which we completed on all epochs separately. To perform MRCSA certain parameters had to be specified: the computation of spectral power occurred within the frequency range of 2 and 22.5 Hz with the frequency resolution set to 0.128 Hz. As mentioned above and in line with Wen and Liu (86), 17 different pairs of resampling factors h and their reciprocals $1/h$ were applied, starting from 1.1 in increments of 0.05 to 1.9. The effective frequency range was determined between 2 and 22.5 Hz, as the effect of any previously used filter persists even after the resampling process, effectively reducing the range for analysis (65). The analysis and the following spectral slope estimation was performed in this frequency range. To procure the estimates of spectral slope β_x and the cross-spectral slope β_{xy}, least squares regression was utilized with log cross-spectral power fitted on log frequency, resulting in 14-by-14 matrices for β_{xy} for every epoch. Additionally, by summing the power between the broadband frequency range's boundaries (2-22.5 Hz) the integrated spectral power was computed, yielding a 14-by-14 matrix per type of spectrum (fractal, oscillatory, mixed) for every epoch. Finally, by averaging matching matrices over the initial 9 epochs we obtained robust estimates for every measure considered in the analysis.

3.3.6 Statistical analysis

Comparisons between the CANTAB scores of the young and elderly cohorts were made using two-sample, unpaired tests. Specifically, Lilliefors test was used to verify the normal distribution of the data. If normality was confirmed, a two-sample t test followed, otherwise a Mann-Whitney U test was performed. Since multiple CANTAB output measures retrieve primarily the same information regarding performance (e.g. number of attempts vs number of errors, median vs mean) the number of comparisons was unnecessarily large ($n_{CANTAB} = 154$). To address this issue, the false discovery rate method (FDR) of Benjamini and Hochberg (111) was employed to adjust the statistical test outcomes.

Fractal connectivity estimates were scrutinized on a connection-by-connection basis using two-sample tests to compare the two groups. This process followed the same statistical principles as outlined with the CANTAB scores. To seek more distinctive differences, the results were subjected to adjustment for multiple comparisons using Bonferroni's method, applied individually for every connectivity measure ($n_{conn} = (14 \cdot 13)/2 = 91$).

Lastly, to explore potential relations, a preliminary analysis was conducted to evaluate if those CANTAB measures that suggested differences in the cognitive performance between young and elderly had any relationship with those connections that showed differences in fractal connectivity between the two groups. To achieve this, we examined the groups individually and calculated the Spearman cross-correlation coefficient between the CANTAB scores and connectivity measures. Note, that the quantity of the comparisons was large ($n_{comb} = 2 \cdot 17 \cdot 54 = 1836$) in contrast with the sample size, thus the results obtained here were not adjusted for multiple comparisons (that would lead to most results being statistically insignificant). Therefore, caution is required when interpreting these results and they should be considered as exploratory.

4 Results

4.1 Effect of increased cognitive load on fractal connectivity

Group-level results regarding β_{xy} and percentage fractal power are shown on **Figures 3.** and **4.**, respectively. In **Figure 3.** it can be observed that word generation resulted in a ubiquitous increase in cross-spectral slope (BL: left panel, WG: middle panel), most prominently in connections involving the frontal and prefrontal cortices. The right panel shows the statistically significant differences ($p<0.05$, Bonferroni-adjusted), with white cells indicating the connections where β_{xy} was significantly different in WG compared to BL. In total, the cross-spectral slope was increased in WG for 143 out of 378 connections. Similar results were obtained for node degree-level analysis (not shown).

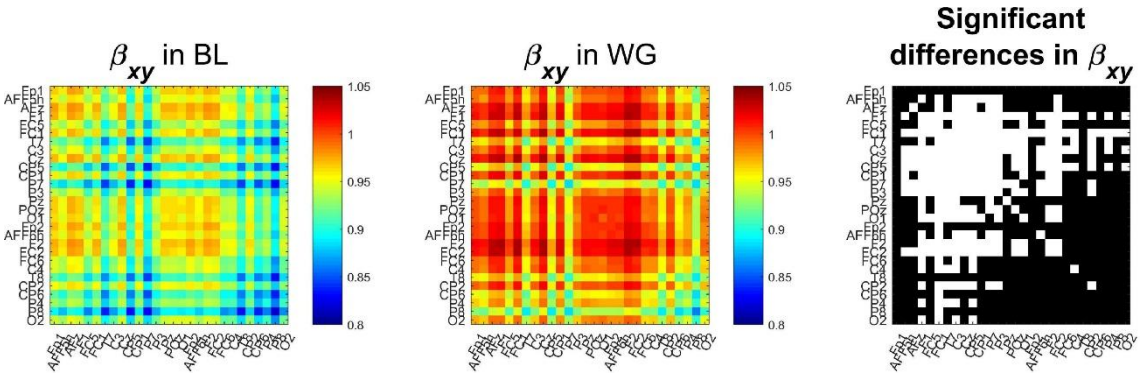

Figure 3. *Cross-spectral slopes of functional connections. In comparison to the baseline condition (left), the cross-spectral slope prominently increases across most connections in word generation (middle). Connections that showed significant differences are highlighted in white on the right panel BL: baseline; WG: word generation (88).*

Percentage of fractal power exhibited a similar pattern (**Figure 4.**); however, most differences were rendered non-significant by multiple comparisons adjustment. In detail, this measure was only significantly different in case of FC1-CP6 connection (p=0,0329), while percentage fractal power was higher over regions FC6 (p=0,0478) and C4 (p=0,0134) in WG compared to BL. Node degree analysis proved to be more sensitive, indicating increased percentage of fractal power in connections of C4, CP6 and P4 regions (p=0,0235, 0,0122 and 0,0478, respectively) in WG when contrasted to BL.

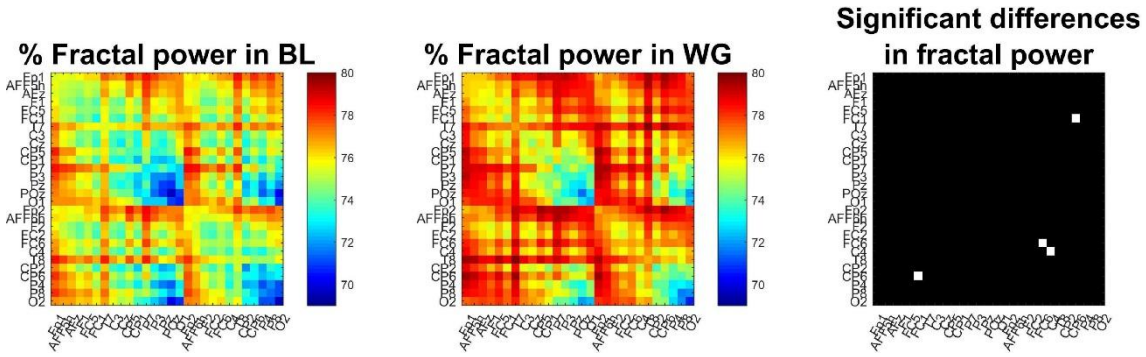

Figure 4. *Ratio of fractal power of functional connections. Generally, the proportion of fractal cross-spectral power appears lower during baseline (left) compared to word generation (middle) condition. Channels indicating a significant increase are highlighted in white on the right panel. Following Bonferroni-adjustment only the connection between FC1 and CP6 showed significant difference. Additionally, higher percentages of fractal auto-spectral power were observed at regions FC6 and C4, as denoted by the two white cells along the main diagonal* (88).

In summary, in this study we demonstrated for the first time that increased mental workload results in a reorganization of fractal brain networks. These results indicated that neural signatures identified with MRCSA analysis capture information that is relevant for cognitive functioning. Therefore, in our subsequent study, our goal was to better understand this phenomenon in a condition that is broadly relevant both in a medical and a socio-economic sense: healthy aging.

4.2 Effects of aging on fractal connectivity and cognition

4.2.1 Behavioral results

In this section, I will present the results of our follow-up study, in which we utilized MRCSA to analyse EEG recordings of healthy young and elderly participants and employed CANTAB to evaluate the cognitive performances. In general, the elderly group had worse performance in generally all cognitive domains investigated (see below). As a

reminder, **Figure 5.** provides a schematic illustration of the CANTAB tasks.

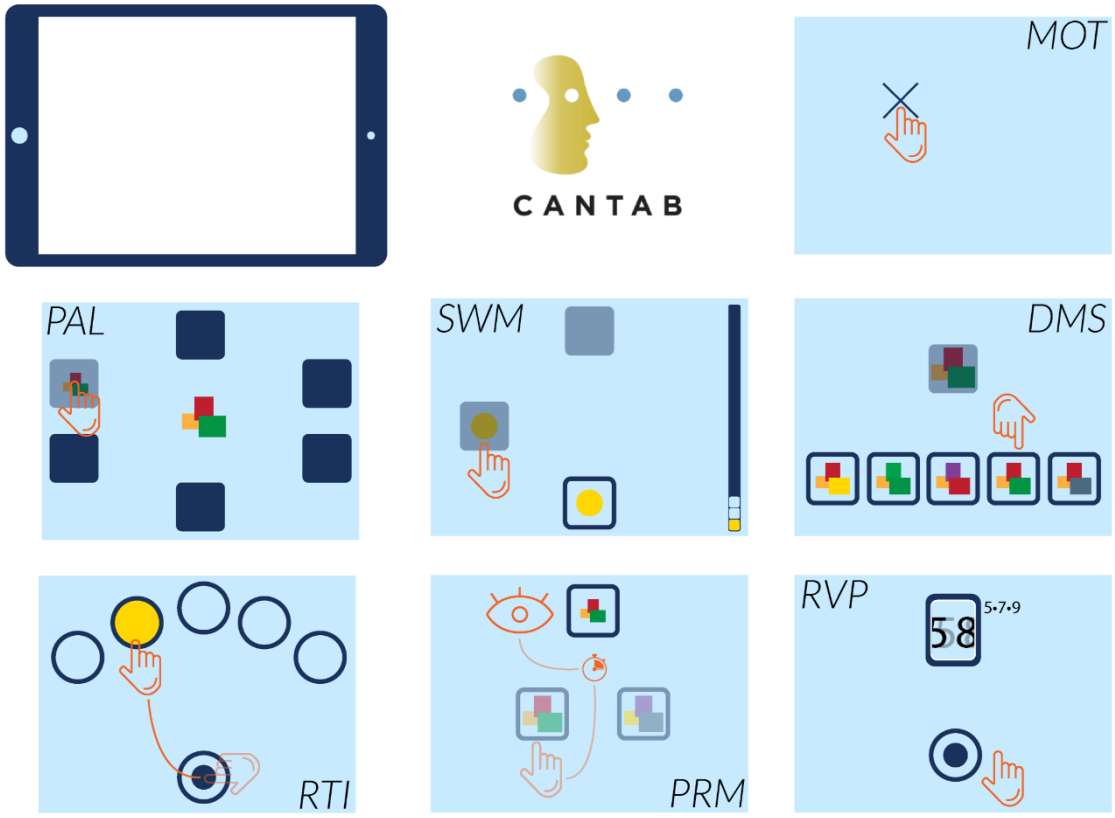

Figure 5. *Schematic illustrations of the CANTAB tasks.* ***MOT****: Motor Screening Task;* ***DMS****: Delayed Matching to Sample;* ***PAL****: Paired Associates Learning;* ***PRM****: Pattern Recognition Memory;* ***RTI****: Reaction Time;* ***RVP****: Rapid Visual Information Processing; SWM: Spatial Working Memory. (Figure made by Zalán Káposzta)*

First, to confirm that the differences in the results were not likely to be caused by the lack of sensorimotor skills, we examined the scores of the MOT task. Here, no significant differences were found, supporting the notion that the participants' sensorimotor skills sufficed to solve the remaining tasks and the emerging differences were not confounded by it. Regarding the other cognitive tests, significant differences were found in 54 cases between the young and elderly group's CANTAB scores after the FDR adjustment. More elaborately, in 10 metrics for DMS, 16 for PAL, 4 for PRM, 4 for RTI, 8 for RVP and 12 for the SWM task.

In the DMS task the participants were shown a visual pattern, then they had to select the previously presented pattern among a set of new ones. These new sets were shown to the participants after predetermined latencies. We found that elderly individuals

responded slower compared to those in the young group when the original pattern and the new set were shown simultaneously (median correct latency, simultaneous, young: 2.2525s, elderly: 3.2389s, p=0.0010) or with the different delays (mean correct latency, all delays, young: 2.4870s, elderly: 3.9567s, p=0.0184). Moreover, the standard deviation of response times increased in the elderly, but only in the 4-s delay variation (p=0.0427). Interestingly, the two groups' performance did not differ significantly, meaning the proportion of correct/erroneous answers were similar.

The most significant contrast between the groups occurred in the PAL task (16 metrics), a test assessing the visuo-spatial memory skills, since the participants had to remember the exact locations of patterns. The results of the elderly group exhibit a universal drop in performance in all task scenarios (recalling the locations of 4, 6, 8 and 12 patterns), however with increasing the difficulty these differences become less distinct. Precisely, the general first attempt memory score (PALFAM28, "*The number of times a subject chose the correct box on their first attempt when recalling the pattern locations. Calculated across assessed trials, omitting 12 box level*") averaged to 16.5417 in the young and 11.9474 in the elderly group (p=0.0004). The number of errors and consequently the number of attempts were found increased in the elderly group in the scenario with 4 (errors: p=0.0251, attempts: p=0.0241), 6 (errors: p=0.0012, attempts: p=0.0013) and 8 (errors: p=0.0314) patterns. In general, the elderly group displayed reduced performance which was more distinct in the easier scenarios with 4 and 6 patterns, but less for the more difficult ones of 8 and 12 patterns.

Third, the PRM task tested the pattern recognition memory. We observed that even though the response time of the elderly were higher in both the immediate (median correct latency, young: 1.2803s, elderly: 1.7440s, p=0.0015) and in the delayed recognition scenarios (median correct latency, young: 1.5310s, elderly: 1.9278s, p=0.0033), the proportion of correct answers did not differ between the groups.

In the RTI task the participants' response time and accuracy were tested with one or five potential targets. Overall, elderly participants were less accurate in their responses (p=0.0244). Additionally, the mean (young: 0.3415s, elderly: 0.3915, p=0.0022) and standard deviation (young: 0.0365s, elderly: 0.0469s, p=0.0228) of response times were found to be greater in the elderly compared to the young group.

Testing sustained attention and working memory, the RVP task results demonstrated greater response times (median latency, young: 0.4115s, elderly: 0.5280s, p=0.0002) and worse performance, calculated regardless of latency from all hits/misses, in the elderly (young: 0.9398, elderly: 0.8971, p=0.0143).

The most elaborate and complex test included in our set was the SWM task. This test assessed spatial working memory skills and task solving strategy. There were 3 different types of mistakes a participant could make: i) between errors, in this case the participant re-checked a box where a token was already found, ii) within errors, where a box that already-proven-empty was re-checked, and iii) total errors, the combination of the two above, meaning they re-checked a box which certainly did not contain a token. We found that in all levels of complexity the elderly performed worse than the young group, manifesting in the increased number of between and total errors (SWMBE468, between errors for 4-6-8 boxes, young: 5, elderly: 19, p=0.0181; SWMBE12 young: 14, elderly: 35, p=0.0082; SWMTE468 total errors for 4-6-8 boxes, young: 6.375, elderly: 15.7895, p=0.0086; SWMTE12 young: 14, elderly: 35, p=0.0113). Moreover, the strategies employed by the elderly in searching for the tokens proved less effective compared to the young participants' (p=0.0241).

In general, the elderly group could be described with greater response time and worse performance compared to the young group. Specifically, no differences emerged in the MOT task, in two tests (RTI and RVP) the increased response latency was associated with reduced performance; on the other hand, with once again two tests (DMS and PRM) the greater response times were accompanied by similar performances when comparing the elderly to the young group. In four tests (DMS, PRM, RTI, and RVP), higher response times were observed, while in another four tests (PAL, RTI, RVP, and SWM), we found that the elderly group underperformed.

4.2.2 Age-related differences in fractal connectivity

In this section I present the results regarding fractal connectivity. We observed 17 connections where the cross-spectral slope proved to be diminished in the elderly group (**Figure 6.**) and seven additional locations where the auto-spectral exponent was reduced, compared to the young group. Overall, the young group could be characterized with higher auto- and cross-spectral slopes (**Figure 6. left panel**) over the whole cortex, but

the significantly different connections were associated mainly with the right temporal and frontal areas. Relatedly, the differences in auto-spectral slopes emerged over the bilateral frontal and temporal areas, and also in the left occipital region (**Figure 6. right panel**).

No differences were found in auto- or cross-spectral power in the fractal, oscillatory or mixed spectra when comparing the two groups.

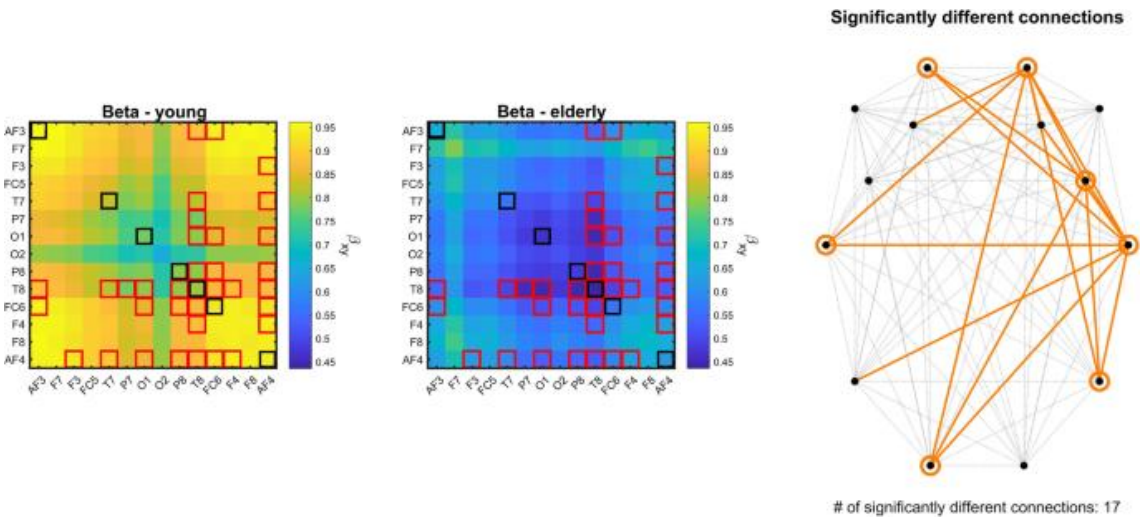

Figure 6. *Auto- and cross-spectral slopes in the young and elderly cohorts. In the left and middle panels, black and red squares indicate the locations or connections where significant differences in the spectral exponent were observed between the two groups. The right panel illustrates the cortical topology of the significant connections and locations. Orange lines shows the connections and circles the locations (107).*

4.2.3 Correlations of fractal connectivity and cognitive function

Finally, our objective was to identify markers linking natural changes in cognition to neurophysiological processes in aging, therefore we narrowed down our analysis to those CANTAB measures and brain connections/areas that were found to be different between the cohorts. The correlation analyses were performed separately on the two groups.

Interestingly, the young group showed only occasional relationships between cognition and fractal connectivity (in the selected subset of features). In more detail, we found the cross-spectral slope β_{xy} in one connection (O1-FC6, r=0.4363, p=0.0330) correlated to the PAL mean error metric and in three connections (O1-AF4, r=0.4070, p= 0.0495; FC6-AF4, r=0.4470, p= 0.0297; F4-AF4, r=0.4200, p=0.0421) with the standard deviation of response latency in the DMS task. Furthermore, the auto-spectral slope β_x of AF4 was found to be correlating with two metrics, namely mean and standard deviation

of latency in DMS (r=0.4409, p=0.0322 and r=0.4861, p=0.0171, respectively), and that of T7 with the standard deviation of five-choice RTI latency (r=-0.4217, p=0.0412).

In contrast, the elderly group showed significant correlations between cross- and auto-spectral slopes and CANTAB metrics. Precisely, in 59 cases with cross-spectral and 26 cases with auto-spectral slopes. After streamlining redundant measures and considering their impact, the bulk of these connections emerged with regards to the RVP performance and PAL performance for 6 patterns.

Figure 7. (left) showcases the connection topology of cross-spectral slope correlation with the RVPA ("*The signal detection measure of a subject's sensitivity to the target sequence (string of three numbers), regardless of response tendency*") metric (7 instances), while rings indicate the regions of the cortex where the auto-spectral slope showed correlations (4 regions). On the right side of **Figure 7.**, blue and yellow scatter-plots demonstrate the correlations found with cross- and auto-spectral slope, respectively. The inverse relationship indicates that a lower spectral slope could be associated with better performance in the RVP task.

A notable outlier is shown on the scatterplots, potentially influencing the results. To investigate its impact, we excluded that participant and repeated the analysis. We found no significant differences in the results (more details can be found in the supplementary material of the original publication (107)). Therefore, the outlier did not account for the observed correlations.

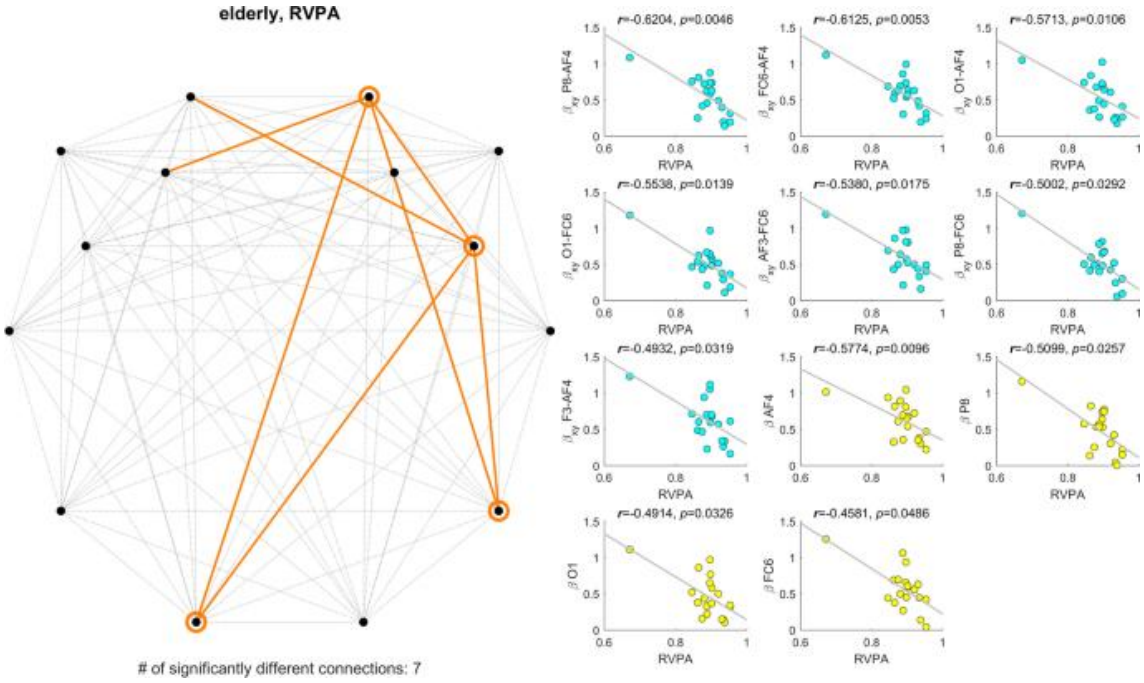

Figure 7. *Significant correlations between spectral slopes and Rapid Visual Processing scores (RVPA). On the left panel, the cortical topology of the significant locations (circles) and connections (lines) are shown, where* β_x *or* β_{xy} *expressed significant correlation with RVPA scores. The right panel displays individual scatterplots for all relationships (yellow:* β_x *vs. RVPA, blue:* β_{xy} *vs. RVPA) (107).*

Figure 8. depicts the relation of the total number of attempts in the 6 pattern PAL task with spectral slopes, in a similar manner as previously. Once again, a greater spectral slope (4 connections and 1 location) was accompanied by more attempts, i.e., worse performance.

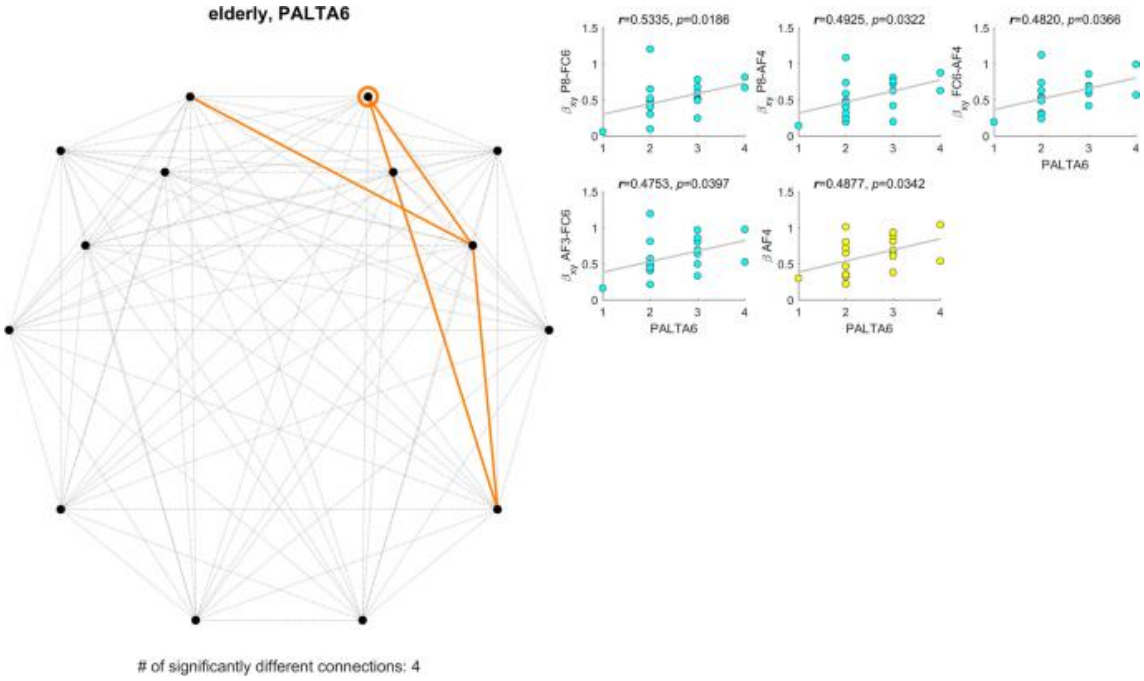

Figure 8. *Significant correlations between spectral slopes and Paired Associates Learning Total Errors in case of 6 patterns (PALTA6). On the left panel are the locations (circles) and connections (orange lines) where* β_x *or* β_{xy} *expressed significant correlation with PALTA6 scores. The right panel displays individual scatterplots for all relationships (yellow:* β_x *vs. PALTA6, blue:* β_{xy} *vs. PALTA6) (107).*

Conforming to expectations, we discovered nearly identical results with regards to the probability of hits in RVP (RVPPH). And similarly with the percentile-transformed and z-scored RVPA values. The other task's CANTAB scores showed only the occasional correlation with fractal connectivity and those results did not present a comprehensible trend or pattern. **Table 2.** shows CANTAB output measures that were found to be different between the groups. All *p*-values reported in **Table 2.Hiba! A hivatkozási forrás nem található.** are adjusted using False Discovery Rate correction of Benjamini and Hochberg (111).

Table 2. *Significant differences in CANTAB scores between young and elderly groups. DMS: Delayed Matching to Sample; PAL: Paired Associates Learning; PRM: Pattern Recognition Memory; RTI: Reaction Time; RVP: Rapid Visual Information Processing; SWM: Spatial Working Memory; SD: standard deviation; CL: correct latency. (modified after the supplementary table of Czoch et al. (107))*

Task	Measure	Definition	Young	Elderly	*p*-value	Task	Measure	Definition	Young	Elderly	*p*-value
DMS	DMSL4SD	Correct latency SD	827.6	1456.7	0.0427	PRM	PRMMCLD	Mean correct latency delayed	1667.1	2082.1	0.0123
	DMSMDL	Median correct latency	2284	3459	0.0122		PRMMCLI	Mean CL immediate	1516.4	1900.7	0.0142
	DMSMDL12	Median correct latency 12	2513.3	3869	0.0097		PRMMDCLD	Median CL delayed	1531	1927.8	0.0033
	DMSMDLAD	Median correct latency all	2287.8	3586	0.0241		PRMMDCLI	Median CL immediate	1280.3	1744	0.0015
	DMSMDLS	Simultaneous DMSMDL	2252.5	3238.9	0.0010	RTI	RTIFMDRT	Median reaction time 5	334.3542	383.7895	0.0022
	DMSML	Mean correct latency	2820.4	3677.5	0.0270		RTIFMRT	Mean reaction time 5	341.5054	391.4468	0.0022
	DMSML12	Mean correct latency 12	2846.1	4322	0.0189		RTIFRTSD	Reaction time 5 SD	36.5422	46.9	0.0228
	DMSML4	Mean correct latency 4	2475.7	3634.2	0.0218	RVP	RVPA	RVP A prime measure	0.9398	0.89871	0.0143
	DMSMLAD	Mean correct latency all	2487	3956.7	0.0184		RVPA%	RVPA percentile	59.9583	36.2632	0.0126
	DMSMLS	Simultaneous DMSML	2403.7	3276.6	0.0033		RVPAZ	RVPA Z-score	0.3454	-0.4242	0.0186
PAL	PALFAMS28	First attempt memory score	16.4517	11.9474	0.0004		RVPMDL	Median response latency	411.5	528	0.0002
	PALFAMS28%	PALFAMS28 percentile	66.5	44.0526	0.0197		RVPML	Mean response latency	466.620	568	0.0010
	PALFAMS28Z	PALFAMS28 Z-score	0.6242	-0.1684	0.0178		RVPPH	Probability of hit	0.7431	0.6140	0.0423
	PALMETS28	Mean errors to success	1	2	0.0013		RVPTH	Total hits	40.1250	33.1579	0.0415
	PALTA28	Total attempts all	6	8	0.0032		RVPTM	Total misses	13.8750	20.8421	0.0407
	PALTA6	Total attempts 6	1	2	0.0013	SWM	SWMBE12	Between errors 12	14	35	0.0082
	PALTE28	Total errors all	5	13.1579	0.0014		SWMBE4	Between errors 4	0	2	0.0192
	PALTE6	Total errors 6	0	3	0.0012		SWMBE468	Between errors 4-6-8	5	19	0.0181
	PALTE8	Total errors 8	4.0417	8.1579	0.0314		SWMBE6	Between errors 6	0	6	0.0277
	PALTEA12	Adjusted PALTE 12	5.5	12	0.0185		SWMS	Strategy score 6-8	6.7083	8.9474	0.0302
	PALTEA28	Adjusted PALTE all	5	13.1579	0.0013		SWMS6	Strategy score 6	3	4	0.0139
	PALTEA6	Adjusted PALTE 6	0	3	0.0010		SWMSX	Strategy score 6-12	11.375	15.5263	0.0241
	PALTEA8	Adjusted PALTE 8	4.0417	8.1579	0.0308		SWMTE12	Total errors 12	14	35	0.0113

5 Discussion

5.1 Fractal connectivity characteristics of different mental states

Our first validation of the MRCSA method on physiological data revealed an increase in cross-spectral exponents of brain networks in response to increased mental workload (as evoked by generating words). Even though this analysis was the first to demonstrate this pattern using this specific methodology, similar results have been observed before: in one of our previous studies (62) we showed that the bivariate Hurst exponent – another measure capturing bivariate fractality of coupled processes – increases when performing a visual pattern recognition task, in accordance with our findings. Even though MRCSA operates in the frequency domain, the bivariate fractal scaling exponent can be obtained equivalently in the frequency- and time domains (57). However, while time domain methods such as detrended cross-correlation analysis (56) cannot account for the biasing effect for oscillatory signal components, MRCSA can ameliorate this issue and thus MRCSA estimates of the bivariate scaling exponent should be considered more precise and robust than those obtained with other techniques. In this regard, our current results (88) confirmed our previous ones (62) in terms of the effect of mental workload on fractal connectivity in the brain. These findings align with theoretical insights into fractal networks, such as those described by Zakar-Polyák et al (112). Their analysis of fractal network models highlights how structural characteristics contribute to fractality. These properties may parallel neural network adaptations under cognitive load, where increased fractal connectivity could reflect a reorganization aimed at optimizing processing efficiency. Their findings suggest that neural networks might transiently adopt more fractal-like configurations during demanding tasks. This perspective provides a robust framework for interpreting our MRCSA-derived measures and underscores the physiological relevance of FrC as a marker for cognitive functioning.

It is important to note that an increase in β_{xy} does not necessarily mean stronger functional coupling, but instead it indicates that the coupling – regardless of its strength – is maintained even for long time scales (99). This phenomenon might be understood in terms of the WG paradigm the following way. The WG task itself requires the alignment of multiple, higher-order cognitive functions such as short- and long-term memory,

associative skills and attention. Furthermore, the task condition was induced for 10 seconds, which might indeed be manifested in long-term coupling as co-operation of these functions (and associated brain regions) had to be maintained throughout the trial. With this hypothesis in mind, we could observe that connections where significant difference was detected compared to resting-state (BL) were associated to those brain regions that are relevant for the aforementioned cognitive domains, such as the prefrontal cortex or constituents of the dorsal- and ventral attention networks (75, 113). However, it must be noted that our analysis was carried out in the electrode (and not the source) space, and therefore conclusions regarding the activity and involvement of underlying brain regions are speculative and should be treated with caution (114).

In addition, the increase in percentage of fractal spectral power indicates a decrease in oscillatory activity. These results might reflect a decrease in oscillatory alpha activity – the most prominent narrow-band component in human EEG –, which suggests a decrease in inhibitory tone and is commonly observed in conditions requiring increased mental workload (115).

5.2 Changes in cognitive performance and response latency in healthy aging

Recent research has increasingly focused on exploring the relationship between age-related cognitive decline and functional connectivity during resting-state (20, 21, 25). Additionally, it has also been described that fractal dynamics is affected by aging (116, 117). Despite the surging interest, most studies in the field focus either solely on 'traditional' connectivity patterns and brain networks or fractal dynamics and how these are altered in certain conditions. We, on the other hand, aimed to combine these concepts and find resting-state fractal connectivity patterns that could be linked to (or even forecast) cognitive performance in the elderly. To test our hypothesis, we completed an extensive assessment concentrating on those cognitive domains which are affected by aging the most (118, 119). We have chosen these seven (along with the MOT task for baseline) tests because it has been demonstrated previously that they are sensitive and efficient in detecting cognitive impairment in aging (120). The results of Csipo and colleagues (120) correspond strongly with our findings. During MOT, the baseline task, the two groups were indistinguishable, verifying that all subject from both cohorts

possessed sufficient sensorimotor skills to complete the remaining tasks. A further similarity was in the DMS task where the response times were higher, and in the PAL, RVP and SWM tasks where we observed the same decrease in performance in the elderly. However, in the former, in our study no reduction of performance accompanied the increased latency and in the latter ones our aging group achieved worse performances as well, compared to the youth. Additionally, our aging group replied slower than the young in the PRM task too, contrasting the outcomes of Csipo et. al (120). On the whole, three deductions can be made from the behavioral results. One, in alignment with earlier findings our results support that this set of cognitive tasks is sensitive, quantifiable and can be efficiently employed in capturing age-related decline in several cognitive domains. Perhaps not surprisingly, but even in the absence of any neuropathological condition the elderly displayed worse performance. Two, excluding the MOT task, the response times of the elderly subjects were typically longer than those of the young group across almost all tasks where it was measured. In two instances, namely in the DMS and PRM tasks which test visual pattern recognition- and short-term visual memory, the elderly displayed comparable performance to the young group. This phenomenon implies that despite the affection or 'aging' of the neural circuits needed to solve the task, elderly participants could compensate the reduced efficiency with increased processing duration. A similar occurrence has been observed in the elderly in error perception and response inhibition tasks (121, 122). Three, also in line with previous results (123, 124), four tasks (PAL, RTI, RVP and SWM, while in RTI and RVP the response latency was increased as well) saw a significant reduction in performance when it came to the elderly. These tests assessed a broad range of cognitive domains, except pattern recognition/matching. Interestingly, two very similar tasks, MOT and RTI produced starkly different results. The RTI task involved a preparatory phase and more options to select the correct one from contrary to MOT where there was only one button to press, but only in the former did we observe increased response time and decreased performance/accuracy in the elderly. Once again, previous studies have found the same phenomenon, that the aging population are more prone to error when forced to react quickly (121). Moreover, also in line with earlier research (125, 126), it could signify that aging affects neurophysiological processes linked to preparation and cued action (which we did not assess in our current study). The SWM task was the most complex task applied in our study. After taking the

redundancy of the outcome measures into account (e.g. the number of attempts increase with the number of errors), this task proved to be most challenging for the elderly compared to the young, as their performance was reduced across all difficulty levels (4, 6, 8 and 12 boxes). This result further backs that increasing task complexity diminishes performance in older adults (127), possibly related to naturally occurring loss of cognitive reserves.

5.3 Changes in fractal connectivity in healthy aging

Overall, the most notable reveal of the fractal connectivity analysis was the reduction of the cross- and auto-spectral slope across the whole cortex (**Figure 6**). Multiple previous studies reporting changes in functional connectivity in aging agree that disconnectivity increases with age (20), which can be linked to cognitive impairment (128). However, it is critical to note that direct comparison of these results is not feasible because the cross-spectral slope/exponent does not translate into the 'strength' of the coupling between the signals. Rather, it indicates how the strength of the coupled processes change over various time scales. Interestingly, comparing integrated cross-spectral density (a more 'conventional' measure of FC), no differences emerged between the groups, contrary to previous findings (129). This difference could be caused by the differing analysis strategies. Here, we only examined broadband spectral power and connection-to-connection comparisons after FDR-adjustment, meanwhile a more comprehensive investigation in the individual frequency ranges combined with network theoretical methods could prove to be more discerning in revealing changes linked to aging. Another study found that aging involves a shift from segregated to integrated functional networks, particularly in the frontal lobe (130). This reorganization aligns with our findings that changes in fractal connectivity (FrC) reflect disruptions in neuronal dynamics across cortical regions. Regardless, our focus was specifically set on FrC and our results prove that evaluating it can reveal age-related changes other, more 'traditional' methods could not. Consequently, as far as we know, no studies had examined FrC in aging and how it might be linked to cognitive performance previously. Prior to MRCSA, our group proposed a novel, parallel approach (for a similar purpose of characterizing fractal connectivity) called bivariate focus-based multifractal formalism (BFMF), to analyse multifractal connectivity (61), in the time domain. In our follow-up papers, with the use of BFMF we demonstrated that FrC is altered in a visual pattern recognition paradigm

(62) and also in Parkinson's Disease and reacts to dopaminergic treatment (131). Despite the implications of these outcomes suggesting a connection between FrC and cognitive performance, none of these studies examined the contrast in FrC between young and healthy elderly groups. Additionally, our goal was not to assess the plausible multifractal nature of connectivity, but instead to obtain precise, unbiased estimates of the (mono)fractal scaling property and thus we utilized the advanced MRCSA instead of the BFMF method. In spite of finding differences linked to aging in FrC, the underlying neurophysiological processes (and fractal neural dynamics in general) are yet to be understood. Based on the neural network oscillator model, larger neuronal assemblies produce slower fluctuations. Thus, the $1/f$ characteristic of neural activity emerges from the overlay of incoming signals from neuronal populations of various sizes (80, 132). Building upon this notion, the decreased cross-spectral slope could very well indicate that disconnectivity emerges in the aging brain affecting neuronal populations to various extents. An additional prevalent hypothesis associates scale-free neural activity with a condition of self-organized criticality in the brain (133), making it capable of global reorganization quickly in reaction to external stimuli (134, 135). As per this concept, altered spectral exponents might indicate changes in the balance of excitatory and inhibitory stimuli (136, 137) and the resulting regional imbalance could very well lead to a desynchronization of various cortical areas across several frequency ranges (138), although further research is required to confirm this theory. Most of the differences in auto- and cross-spectral exponents were concentrated on the frontal and temporal regions (right panel of **Figure 6**). This can be explained by that the univariate spectral slope can in fact determine the bivariate scaling exponent (99). Our findings on fractal connectivity changes in healthy aging align with recent research on functional brain network alterations across the lifespan. A comprehensive study by Doval et al. (139) using magnetoencephalography data from 792 healthy individuals revealed significant shifts in functional connectivity patterns across multiple frequency bands. Notably, they observed decreased connectivity in the elderly group, particularly in occipital regions and their connections with hippocampal and parahippocampal areas in the delta band, and a widespread decrease in theta connectivity. These patterns support the notion that aging involves specific regional changes in neural dynamics. Moreover, the identified involvement of the frontotemporal network in aging is consistent with previous research

(140, 141), and is further supported by the findings of Doval et al. of altered connectivity in frontal and temporal regions across various frequency bands, particularly in the alpha and gamma ranges (139).

5.4 Associations between fractal connectivity and cognitive abilities in older adults

The most numerous correlations of FrC and performance emerged in the RVP and PAL tasks (**Figure 7.** and **Figure 8.**). The RVP task assessed the sustained attention skills of the participants. The task interface is very similar to the widely favoured n-back working memory paradigm (142). In contrast with n-back, the subjects had to identify one (or more) previously fixed sequence, without updating it every trial. Among cognitive domains, working memory stands out as one of the earliest to be affected by aging, as indicated by prior research (143), thus it is not unexpected to find that a similar task produced the most correlations with neural signatures. Moreover, studies agree that the frontal and prefrontal areas (e.g. the dorsolateral prefrontal cortex) play an important role in working memory and sustained attention (69, 144, 145). This is further supported by the correlations found between regional spectral exponents of these areas and performance in RVP. The PAL task, which assessed visual memory and learning, saw an analogous pattern related to the number of attempts emerging. Earlier it has been shown that the cortical regions responsible for visual memory go through a reorganization with aging (146), however differences in performance between young and elderly have not been scrutinized. In contrast, our findings suggest that when long term coupling occurs between the frontal and parietal brain areas, it hinders the continuity of visual memory. Precisely, this is indicated by the reduced auto- and cross-spectral slopes found in the aging group. Interestingly, an inverse relationship **(Figure 7.)** was uncovered between spectral slopes and RVP score (the greater, the better), and additionally, a positive relationship **(Figure 8.)** between the spectral slopes and the number of attempts at PAL (the lower slope, the better the performance). Recent findings from Jauny et al. (2024) (147) show that lower structural-functional connectivity similarity in parietal and temporal regions correlates with better cognitive performance in older adults. This aligns with our observation that reduced spectral slopes may reflect compensatory mechanisms, suggesting FrC changes represent adaptive reorganization rather than decline. As the

young group had an overall better performance, it is somewhat remarkable that they also exhibited higher spectral slopes, therefore one could connect the higher β_x and β_{xy} values to sharper cognitive abilities. Note that in spite of this, nearly none of the cognitive scores showed correlations with spectral exponents in the young cohort, hence universal associations cannot be made and the observed correlations in the elderly should not be dismissed. Rather, the gathered data implies that there might be a (yet unknown) compensatory mechanism in the aging brain as a response to diminished cognitive capabilities, which manifests as a reduction in spectral exponents. Regardless, these questions were ultimately beyond the scope of our study and require further research.

5.5 The physiological role of fractal connectivity

The exact role and meaning of fractal connectivity – and fractal neural activity – is still a subject of debate and active research among the neuroscience community. On the one hand, the functional relevance of fractal neural dynamics has been demonstrated in a plethora of conditions, such as mental workload (51, 78, 148, 149), self-consciousness (150, 151) or anxiety (152). Even though exact generating mechanisms were not identified in most cases, the robust changes observed in spectral slope (or Hurst exponent) indicates that processes governing fractal scaling are task relevant. Recent research proposed that the spectral exponent might reflect the ratio of incoming excitatory and inhibitory signalling to a given region (153), which is a similar notion to the one proposed by Ivanov and colleagues (154) to explain the emergence of fractal dynamics in the presence of non-linear, antagonistic feedback loops. On the other hand, the ubiquitous nature of fractal '$1/f$' dynamics in many natural processes provides a reason for scepticism (155, 156), and thus many approaches consider fractal neural dynamics simply as '$1/f$ noise'(157). Nevertheless, most previous approaches considered fractal characteristics of regional neural dynamics, while studies assessing fractal connectivity are scarce (53, 60, 61, 70), especially those doing so in response to a cognitive task (54, 62). In my work, I provided two arguments supporting the physiological role and relevance of fractal connectivity. First, I showed that fractal connectivity patterns change in response to a mental workload task, and these changes appear to be aligned with task-relevant functional brain regions. Second, I showed that not only fractal connectivity (and regional fractal dynamics) decreases with age, but this alteration is correlated with

cognitive performance in multiple domains. Although the exact neural mechanisms behind these findings could not be disentangled with our experimental setup and limitations, investigating fractal connectivity nevertheless appears as an interesting and relevant direction for future neuroscience research.

5.6 Limitations and future perspectives

Despite the fact that MRCSA can effectively separate the fractal constituent from the cross-power spectrum, some prior assumptions must be made at its application, as mentioned above. Regardless, future theoretical and technical advancements could potentially address or expand upon certain limitations of the method presented here. Also, MRCSA might be extendable to the bimodal domain, based on the works of Nagy et al. (158) and Mukli et al. (68). Moreover, fractal processes in nature can rarely be characterized with one scaling exponent since the scaling property itself can change over time. To provide a solution, Benzi et al. (159) and Mandelbrot (160) proposed a phenomenon termed *multifractality*, that instead of one, a set of exponents should be estimated in these cases. Various processes in physiology exhibit multifractality such as heart rate variability (161) or cerebral hemodynamics (162). More importantly, functional connectivity has been shown to exhibit multifractal dynamics in terms of the topological properties of the overall network (71, 76) and also in individual connections (61, 62, 72). The MRCSA method as presented here is only able to describe the global *monofractal* character of functional coupling, however a sliding window approach could prove useful in obtaining a distribution of local cross-spectral exponents over time, then the degree of multifractality could be computed from the distribution width. Finally, MRCSA could be an effective tool in other fields than neuroscience, as well. In financial data analysis, assessing long-term coupling is gaining traction (56, 163), as these time series express long-range auto- and cross-correlations, interspersed with periodic peaks (monthly/yearly periods or cycles). MRCSA effectively eliminates the interference of multiple periodic elements simultaneously, thus it has the potential to serve as a valuable tool in financial data analysis as well.

Furthermore, MRCSA is computationally very costly method, thus online applications are not feasible. If one intends to monitor cognitive states in real-time, the newly proposed real-time detrended cross-correlation analysis (164) provides an

alternative solution. Lastly, in my work the focus was on identifying biomarkers which are connected to changes in brain networks in healthy aging. Consequently, a significant challenge lies in distinguishing between the natural changes that accompany aging and those that are typical in certain pathological conditions – like mild cognitive impairment or Alzheimer's Disease – is a challenge for the future, albeit an equally important one. Therefore, among our future objectives, we aim to explore the relationship between cognition and FrC in pertinent clinical conditions.

6 Conclusions

During my work, we proposed and developed the bivariate extension of IRASA, called MRCSA, for isolating the fractal component of a cross-spectra of long-term coupled signals. We demonstrated that MRCSA is a potent method to eliminate oscillatory or narrow-band peaks from the cross-power spectrum. We showcased the relevancy of MRCSA on real-world EEG recordings and how the obtained cross-spectral slopes could be employed in differentiating between resting state and increased mental workload. Moreover, MRCSA could prove useful in other disciplines where periodic patterns pose a similar difficulty as narrow-band oscillations in neurophysiological signals, for instance in financial data analysis.

After validating the method, I set out to investigate resting-state fractal connectivity in healthy elderly and young participants and scrutinized its connections with cognitive performance and compared the results of the two groups. The cognitive evaluation showed an increase in response time and decreased performance in the elderly in several tasks, concurrent with an overall reduction in local and cross-regional spectral exponents. Analyzing the correlations, it was found that performance showed an inverse relationship with fractal connectivity dynamics in the elderly. Such reduction in FrC is likely the manifestation of compensating for decreased cognitive abilities. These results are the first to uncover alterations in fractal connectivity connected to aging and their associations to cognitive functioning, and thus will lay the groundwork for future studies focused on employing these markers for monitoring, screening or potential intervention.

7 Summary

I investigated the relationship between fractal connectivity and cognitive functions within the context of healthy aging. My primary objective was to uncover how age-related alterations in brain connectivity patterns influenced cognitive abilities. Firstly, I delved into fractal connectivity (FrC), which represents the self-similar patterns of brain activity crucial for cognitive performance. To estimate and analyze FrC our lab developed a method termed Multiple-Resampling Cross-Spectral Analysis (MRCSA), the bivariate extension of Irregular-Resampling Auto-Spectral Analysis (IRASA). This technique allowed for an unbiased estimation of the spectral slope, which characterizes fractal connectivity. Secondly, to test cognitive performance I utilized tasks from the Cambridge Neuropsychological Test Automated Battery (CANTAB) to assess various cognitive domains. These tests provided comprehensive insights into visual memory, attention, reaction time, and problem-solving abilities. The impact of aging on fractal connectivity and cognitive performance formed the third focal area of my study. I investigated age-related differences in connectivity patterns and their correlations with cognitive test outcomes. The results revealed that healthy aging was associated with distinct changes in fractal connectivity, which might be the underlying cause for the observed decline in specific cognitive capabilities. To ensure statistical robustness, the False Discovery Rate (FDR) method was employed to adjust the number of comparisons in the case of CANTAB and Bonferroni's method of multiple comparisons with the connectivity metrics. The results of my study indicated that increased cognitive load affected FrC differently in younger and older adults. Healthy elderly individuals displayed distinct connectivity patterns compared to younger participants, and these patterns correlated with their cognitive performance. I identified significant age-related differences in fractal connectivity linked to specific cognitive domains, highlighting the potential of FrC as a biomarker for cognitive aging. It must be stressed that further research is needed to explore potential therapeutic interventions that could mitigate age-related cognitive decline. In conclusion, my dissertation established that FrC plays a crucial role in cognitive functioning, and its alteration with age might contribute to cognitive decline. By understanding the neural mechanisms underlying age-related cognitive changes, we could develop more effective strategies to support cognitive longevity.

8 References

1. Wandell BA, Dumoulin SO, Brewer AA. Visual field maps in human cortex. Neuron. 2007;56(2):366-383.

2. Squire LR, Stark CE, Clark RE. The medial temporal lobe. Annu Rev Neurosci. 2004;27:279-306.

3. Miller EK, Cohen JD. An integrative theory of prefrontal cortex function. Annual review of neuroscience. 2001;24:167-202.

4. Alvarez JA, Emory E. Executive Function and the Frontal Lobes: A Meta-Analytic Review. Neuropsychology Review. 2006;16(1):17-42.

5. Friston KJ. Functional and effective connectivity: a review. Brain Connect. 2011;1(1):13-36.

6. Bressler SL, Menon V. Large-scale brain networks in cognition: emerging methods and principles. Trends in cognitive sciences. 2010;14(6):277-290.

7. Raichle ME, MacLeod AM, Snyder AZ, Powers WJ, Gusnard DA, Shulman GL. A default mode of brain function. PNAS. 2001;98(2):676-682.

8. Fox MD, Snyder AZ, Vincent JL, Corbetta M, Van Essen DC, Raichle ME. The human brain is intrinsically organized into dynamic, anticorrelated functional networks. PNAS. 2005;102(27):9673-9678.

9. Szczepanski SM, Pinsk MA, Douglas MM, Kastner S, Saalmann YB. Functional and structural architecture of the human dorsal frontoparietal attention network. PNAS. 2013;110(39):15806-15811.

10. Folkow B, Svanborg A. Physiology of Cardiovascular Aging. Physiol Rev. 1993;73(4):725-764.

11. Kirkendall DT, Garrett WE. The effects of aging and training on skeletal muscle. Am J Sport Med. 1998;26(4):598-602.

12. Sharma G, Goodwin J. Effect of aging on respiratory system physiology and immunology. Clin Interv Aging. 2006;1(3):253-260.

13. Murman DL. The Impact of Age on Cognition. Semin Hear. 2015;36(3):111-121.

14. Salthouse TA. Selective review of cognitive aging. J Int Neuropsych Soc. 2010;16(5):754-760.

15. Glisky EL. Changes in Cognitive Function in Human Aging. In: Riddle DR, editor. Brain Aging: Models, Methods, and Mechanisms. Frontiers in Neuroscience. Boca Raton (FL)2007.

16. Pettigrew C, Martin RC. Cognitive declines in healthy aging: evidence from multiple aspects of interference resolution. Psychol Aging. 2014;29(2):187-204.

17. Pichora-Fuller MK, Mick P, Reed M. Hearing, Cognition, and Healthy Aging: Social and Public Health Implications of the Links between Age-Related Declines in Hearing and Cognition. Semin Hear. 2015;36(3):122-139.

18. Roalf DR, Moberg PJ, Xie SX, Wolk DA, Moelter ST, Arnold SE. Comparative accuracies of two common screening instruments for classification of Alzheimer's disease, mild cognitive impairment, and healthy aging. Alzheimers Dement. 2013;9(5):529-537.

19. Bishop NA, Lu T, Yankner BA. Neural mechanisms of ageing and cognitive decline. Nature. 2010;464(7288):529-535.

20. Ferreira LK, Busatto GF. Resting-state functional connectivity in normal brain aging. Neurosci Biobehav R. 2013;37(3):384-400.

21. Sala-Llonch R, Bartres-Faz D, Junque C. Reorganization of brain networks in aging: a review of functional connectivity studies. Frontiers in psychology. 2015;6:663.

22. Damoiseaux JS. Effects of aging on functional and structural brain connectivity. Neuroimage. 2017;160:32-40.

23. Reuter-Lorenz PA, Cappell KA. Neurocognitive aging and the compensation hypothesis. Curr Dir Psychol Sci. 2008;17(3):177-182.

24. Sala-Llonch R, Arenaza-Urquijo EM, Valls-Pedret C, Vidal-Pineiro D, Bargallo N, Junque C, Bartres-Faz D. Dynamic functional reorganizations and relationship with working memory performance in healthy aging. Front Hum Neurosci. 2012;6:152.

25. Onoda K, Ishihara M, Yamaguchi S. Decreased Functional Connectivity by Aging Is Associated with Cognitive Decline. J Cognitive Neurosci. 2012;24(11):2186-2198.

26. Hirsiger S, Koppelmans V, Merillat S, Liem F, Erdeniz B, Seidler RD, Jancke L. Structural and functional connectivity in healthy aging: Associations for cognition and motor behavior. Hum Brain Mapp. 2016;37(3):855-867.

27. Hausman HK, O'Shea A, Kraft JN, Boutzoukas EM, Evangelista ND, Van Etten EJ, Bharadwaj PK, Smith SG, Porges E, Hishaw GA, Wu S, DeKosky S, Alexander GE, Marsiske M, Cohen R, Woods AJ. The Role of Resting-State Network Functional Connectivity in Cognitive Aging. Front Aging Neurosci. 2020;12.

28. Stam CJ. Modern network science of neurological disorders. Nat Rev Neurosci. 2014;15(10):683-695.

29. Lal U, Chikkankod AV, Longo L. Fractal dimensions and machine learning for detection of Parkinson's disease in resting-state electroencephalography. Neural Computing and Applications. 2024;36(15):8257-8280.

30. Lin Q, Rosenberg MD, Yoo K, Hsu TW, O'Connell TP, Chun MM, Initi ADN. Resting-State Functional Connectivity Predicts Cognitive Impairment Related to Alzheimer's Disease. Front Aging Neurosci. 2018;10.

31. Dubbelink KTEO, Hillebrand A, Stoffers D, Deijen JB, Twisk JWR, Stam CJ, Berendse HW. Disrupted brain network topology in Parkinson's disease: a longitudinal magnetoencephalography study. Brain. 2014;137:197-207.

32. Bajo R, Maestu F, Nevado A, Sancho M, Gutierrez R, Campo P, Castellanos NP, Gil P, Moratti S, Pereda E, del-Pozo F. Functional Connectivity in Mild Cognitive Impairment During a Memory Task: Implications for the Disconnection Hypothesis. J Alzheimers Dis. 2010;22(1):183-193.

33. Rissman J, Gazzaley A, D'Esposito M. Measuring functional connectivity during distinct stages of a cognitive task. Neuroimage. 2004;23(2):752-763.

34. Racz FS, Mukli P, Nagy Z, Eke A. Increased prefrontal cortex connectivity during cognitive challenge assessed by fNIRS imaging. Biomed Opt Express. 2017;8(8):3842-3855.

35. O'Neill GC, Tewarie PK, Colclough GL, Gascoyne LE, Hunt BAE, Morris PG, Woolrich MW, Brookes MJ. Measurement of dynamic task related functional networks using MEG. Neuroimage. 2017;146:667-678.

36. Dimitrakopoulos GN, Kakkos I, Dai ZX, Lim J, deSouza JJ, Bezerianos A, Sun Y. Task-Independent Mental Workload Classification Based Upon Common Multiband EEG Cortical Connectivity. Ieee T Neur Sys Reh. 2017;25(11):1940-1949.

37. Kaposzta Z, Stylianou O, Mukli P, Eke A, Racz F. Decreased connection density and modularity of functional brain networks during n-back working memory paradigm. Brain and Behavior. 2020:e01932-e01932.

38. Friston KJ. The labile brain. II. Transients, complexity and selection. Philos Trans R Soc Lond B Biol Sci. 2000;355(1394):237-252.

39. Gómez-Lombardi A, Costa BG, Gutiérrez PP, Carvajal PM, Rivera LZ, El-Deredy W. The cognitive triad network - oscillation - behaviour links individual differences in EEG theta frequency with task performance and effective connectivity. Sci Rep-Uk. 2024;14(1):21482.

40. Hou FZ, Liu C, Yu ZN, Xu XD, Zhang JY, Peng CK, Wu CY, Yang A. Age-Related Alterations in Electroencephalography Connectivity and Network Topology During n-Back Working Memory Task. Frontiers in Human Neuroscience. 2018;12.

41. Tanaka M, Yamada E, Mori F. Neurophysiological markers of early cognitive decline in older adults: a mini-review of electroencephalography studies for precursors of dementia. Front Aging Neurosci. 2024;16.

42. Nagel IE, Preuschhof C, Li SC, Nyberg L, Backman L, Lindenberger U, Heekeren HR. Load Modulation of BOLD Response and Connectivity Predicts Working Memory Performance in Younger and Older Adults. J Cognitive Neurosci. 2011;23(8):2030-2045.

43. Cao J, Zhao Y, Shan X, Wei H-l, Guo Y, Chen L, Erkoyuncu JA, Sarrigiannis PG. Brain functional and effective connectivity based on electroencephalography recordings: A review. Hum Brain Mapp. 2022;43(2):860-879.

44. Di Gregorio F, Battaglia S. Advances in EEG-based functional connectivity approaches to the study of the central nervous system in health and disease. Adv Clin Exp Med. 2023;32(6):607-612.

45. Perinelli A, Assecondi S, Tagliabue CF, Mazza V. Power shift and connectivity changes in healthy aging during resting-state EEG. NeuroImage. 2022;256:119247.

46. Javaid H, Kumarnsit E, Chatpun S. Age-Related Alterations in EEG Network Connectivity in Healthy Aging. Brain Sciences. 2022;12(2):218.

47. Mandelbrot B. The Fractal Geometry of Nature. New York: W. H. Freeman and Co; 1983.

48. Campillo M, Paul A. Long-range correlations in the diffuse seismic coda. Science. 2003;299(5606):547-549.

49. Marinho EBS, Sousa AMYR, Andrade RFS. Using Detrended Cross-Correlation Analysis in geophysical data. Physica A. 2013;392(9):2195-2201.

50. Vassoler RT, Zebende GF. DCCA cross-correlation coefficient apply in time series of air temperature and air relative humidity. Physica A. 2012;391(7):2438-2443.

51. He BJ. Scale-free properties of the functional magnetic resonance imaging signal during rest and task. J Neurosci. 2011;31(39):13786-13795.

52. Podobnik B, Horvatic D, Ng AL, Stanley HE, Ivanov PC. Modeling long-range cross-correlations in two-component ARFIMA and FIARCH processes. Physica A. 2008;387(15):3954-3959.

53. Achard S, Bassett DS, Meyer-Lindenberg A, Bullmore ET. Fractal connectivity of long-memory networks. Phys Rev E. 2008;77(3).

54. Ciuciu P, Abry P, He BJ. Interplay between functional connectivity and scale-free dynamics in intrinsic fMRI networks. Neuroimage. 2014;95:248-263.

55. Grosu GF, Hopp AV, Moca VV, Bârzan H, Ciuparu A, Ercsey-Ravasz M, Winkel M, Linde H, Mureșan RC. The fractal brain: scale-invariance in structure and dynamics. Cereb Cortex. 2022;33(8):4574-4605.

56. Podobnik B, Stanley HE. Detrended cross-correlation analysis: a new method for analyzing two nonstationary time series. Physical review letters. 2008;100(8):084102.

57. Kristoufek L. Spectrum-based estimators of the bivariate Hurst exponent. Phys Rev E. 2014;90(6).

58. Eke A, Herman P, Bassingthwaighte JB, Raymond GM, Percival DB, Cannon M, Balla I, Ikrenyi C. Physiological time series: distinguishing fractal noises from motions. Pflugers Arch. 2000;439(4):403-415.

59. Eke A, Herman P, Kocsis L, Kozak LR. Fractal characterization of complexity in temporal physiological signals. Physiol Meas. 2002;23(1):1-38.

60. La Rocca D, Wendt H, van Wassenhove V, Ciuciu P, Abry P. Revisiting Functional Connectivity for Infraslow Scale-Free Brain Dynamics Using Complex Wavelets. Front Physiol. 2021;11.

61. Stylianou O, Racz FS, Eke A, Mukli P. Scale-Free Coupled Dynamics in Brain Networks Captured by Bivariate Focus-Based Multifractal Analysis. Front Physiol. 2020;11:615961.

62. Stylianou O, Racz FS, Kim K, Kaposzta Z, Czoch A, Yabluchanskiy A, Eke A, Mukli P. Multifractal Functional Connectivity Analysis of Electroencephalogram Reveals Reorganization of Brain Networks in a Visual Pattern Recognition Paradigm. Front Hum Neurosci. 2021;15:740225.

63. Denier N, Grieder M, Jann K, Breit S, Mertse N, Walther S, Soravia LM, Meyer A, Federspiel A, Wiest R, Bracht T. Analyzing fractal dimension in electroconvulsive therapy: Unraveling complexity in structural and functional neuroimaging. NeuroImage. 2024;297:120671.

64. He BYJ. Scale-free brain activity: past, present, and future. Trends in cognitive sciences. 2014;18(9):480-487.

65. Racz FS, Farkas K, Stylianou O, Kaposzta Z, Czoch A, Mukli P, Csukly G, Eke A. Separating scale-free and oscillatory components of neural activity in schizophrenia. Brain Behav. 2021;11(5):e02047.

66. Eke A, Herman P, Hajnal M. Fractal and noisy CBV dynamics in humans: influence of age and gender. Journal of cerebral blood flow and metabolism : official journal of the International Society of Cerebral Blood Flow and Metabolism. 2006;26(7):891-898.

67. Churchill NW, Spring R, Grady C, Cimprich B, Askren MK, Reuter-Lorenz PA, Jung MS, Peltier S, Strother SC, Berman MG. The suppression of scale-free fMRI brain dynamics across three different sources of effort: aging, task novelty and task difficulty. Sci Rep-Uk. 2016;6.

68. Mukli P, Nagy Z, Racz FS, Herman P, Eke A. Impact of Healthy Aging on Multifractal Hemodynamic Fluctuations in the Human Prefrontal Cortex. Front Physiol. 2018;9.

69. Seeburger DT, Xu N, Ma M, Larson S, Godwin C, Keilholz SD, Schumacher EH. Time-varying functional connectivity predicts fluctuations in sustained attention in a serial tapping task. Cognitive, affective & behavioral neuroscience. 2024;24(1):111-125.

70. Wang J, Zhao DQ. Detrended cross-correlation analysis of electroencephalogram. Chinese Phys B. 2012;21(2).

71. Racz FS, Mukli P, Nagy Z, Eke A. Multifractal dynamics of resting-state functional connectivity in the prefrontal cortex. Physiol Meas. 2018;39(2):024003.

72. Racz FS, Stylianou O, Mukli P, Eke A. Multifractal Dynamic Functional Connectivity in the Resting-State Brain. Front Physiol. 2018;9:1704.

73. Stam CJ, de Bruin EA. Scale-free dynamics of global functional connectivity in the human brain. Hum Brain Mapp. 2004;22(2):97-109.

74. Van de Ville D, Britz J, Michel CM. EEG microstate sequences in healthy humans at rest reveal scale-free dynamics. PNAS. 2010;107(42):18179-18184.

75. Racz FS, Stylianou O, Mukli P, Eke A. Multifractal and entropy analysis of resting-state electroencephalography reveals spatial organization in local dynamic functional connectivity. Sci Rep-Uk. 2019;9.

76. Racz FS, Stylianou O, Mukli P, Eke A. Multifractal and Entropy-Based Analysis of Delta Band Neural Activity Reveals Altered Functional Connectivity Dynamics in Schizophrenia. Front Syst Neurosci. 2020;14.

77. Kristoufek L. Multifractal height cross-correlation analysis: A new method for analyzing long-range cross-correlations. Epl-Europhys Lett. 2011;95(6).

78. He BJ, Zempel JM, Snyder AZ, Raichle ME. The temporal structures and functional significance of scale-free brain activity. Neuron. 2010;66(3):353-369.

79. Gonzalez J, Gamundi A, Rial R, Nicolau MC, De Vera L, Pereda E. Nonlinear, fractal, and spectral analysis of the EEG of lizard, Gallotia galloti. Am J Physiol-Reg I. 1999;277(1):R86-R93.

80. Buzsaki G, Draguhn A. Neuronal oscillations in cortical networks. Science. 2004;304(5679):1926-1929.

81. Buzsaki G, Anastassiou CA, Koch C. The origin of extracellular fields and currents - EEG, ECoG, LFP and spikes. Nat Rev Neurosci. 2012;13(6):407-420.

82. Murias M, Webb SJ, Greenson J, Dawson G. Resting state cortical connectivity reflected in EEG coherence in individuals with autism. Biol Psychiatry. 2007;62(3):270-273.

83. Yamamoto Y, Hughson RL. Coarse-Graining Spectral-Analysis - New Method for Studying Heart-Rate-Variability. J Appl Physiol. 1991;71(3):1143-1150.

84. Yamamoto Y, Hughson RL. Extracting Fractal Components from Time-Series. Physica D. 1993;68(2):250-264.

85. Mandelbrot BB, Van Ness JW. Fractional Brownian motions, fractional noises and applications. SIAM review. 1968;10(4):422-437.

86. Wen HG, Liu ZM. Separating Fractal and Oscillatory Components in the Power Spectrum of Neurophysiological Signal. Brain Topogr. 2016;29(1):13-26.

87. Murias M, Swanson JM, Srinivasan R. Functional connectivity of frontal cortex in healthy and ADHD children reflected in EEG coherence. Cereb Cortex. 2007;17(8):1788-1799.

88. Racz FS, Czoch A, Kaposzta Z, Stylianou O, Mukli P, Eke A. Multiple-Resampling Cross-Spectral Analysis: An Unbiased Tool for Estimating Fractal Connectivity With an Application to Neurophysiological Signals. Front Physiol. 2022;13.

89. Mandelbrot BB, Wallis JR. Computer Experiments With Fractional Gaussian Noises: Part 1, Averages and Variances. Water Resources Research. 1969;5(1):228-241.

90. Linkenkaer-Hansen K, Nikouline VV, Palva JM, Ilmoniemi RJ. Long-range temporal correlations and scaling behavior in human brain oscillations. J Neurosci. 2001;21(4):1370-1377.

91. Podobnik B, Fu DF, Stanley HE, Ivanov PC. Power-law autocorrelated stochastic processes with long-rangecross-correlations. The European Physical Journal B. 2007;56(1):47-52.

92. Zhou WX. Multifractal detrended cross-correlation analysis for two nonstationary signals. Physical review E, Statistical, nonlinear, and soft matter physics. 2008;77(6 Pt 2):066211.

93. Arianos S, Carbone A. Cross-correlation of long-range correlated series. J Stat Mech-Theory E. 2009.

94. Kristoufek L. Fractal approach towards power-law coherency to measure cross-correlations between time series. Commun Nonlinear Sci. 2017;50:193-200.

95. Podobnik B, Jiang ZQ, Zhou WX, Stanley HE. Statistical tests for power-law cross-correlated processes. Phys Rev E. 2011;84(6).

96. Kristoufek L. Mixed-correlated ARFIMA processes for power-law cross-correlations. Physica A. 2013;392(24):6484-6493.

97. Kristoufek L. Testing power-law cross-correlations: rescaled covariance test. Eur Phys J B. 2013;86(10).

98. Sela RJ, Hurvich CM. The averaged periodogram estimator for a power law in coherency. J Time Ser Anal. 2012;33(2):340-363.

99. Kristoufek L. Can the bivariate Hurst exponent be higher than an average of the separate Hurst exponents? Physica A. 2015;431:124-127.

100. Bassett GW. Equivariant, Monotonic, 50-Percent Breakdown Estimators. Am Stat. 1991;45(2):135-137.

101. Shin J, von Luhmann A, Kim DW, Mehnert J, Hwang HJ, Muller KR. Data Descriptor: Simultaneous acquisition of EEG and NIRS during cognitive tasks for an open access dataset. Sci Data. 2018;5.

102. Oostenveld R, Praamstra P. The five percent electrode system for high-resolution EEG and ERP measurements. Clin Neurophysiol. 2001;112(4):713-719.

103. Delorme A, Makeig S. EEGLAB: an open source toolbox for analysis of single-trial EEG dynamics including independent component analysis. J Neurosci Methods. 2004;134(1):9-21.

104. Winkler I, Haufe S, Tangermann M. Automatic Classification of Artifactual ICA-Components for Artifact Removal in EEG Signals. Behav Brain Funct. 2011;7.

105. Winkler I, Brandl S, Horn F, Waldburger E, Allefeld C, Tangermann M. Robust artifactual independent component classification for BCI practitioners. J Neural Eng. 2014;11(3).

106. Rubinov M, Sporns O. Complex network measures of brain connectivity: Uses and interpretations. NeuroImage. 2010;52(3):1059-1069.

107. Czoch A, Kaposzta Z, Mukli P, Stylianou O, Eke A, Racz FS. Resting-state fractal brain connectivity is associated with impaired cognitive performance in healthy aging. GeroScience. 2024;46(1):473-489.

108. Gabard-Durnam LJ, Leal ASM, Wilkinson CL, Levin AR. The Harvard Automated Processing Pipeline for Electroencephalography (HAPPE): Standardized Processing Software for Developmental and High-Artifact Data. Front Neurosci. 2018;12:97.

109. Csipo T, Mukli P, Lipecz A, Tarantini S, Bahadli D, Abdulhussein O, Owens C, Kiss T, Balasubramanian P, Nyul-Toth A, Hand RA, Yabluchanska V, Sorond FA, Csiszar A, Ungvari Z, Yabluchanskiy A. Assessment of age-related decline of neurovascular coupling responses by functional near-infrared spectroscopy (fNIRS) in humans. Geroscience. 2019;41(5):495-509.

110. Boutros NN, Arfken C, Galderisi S, Warrick J, Pratt G, Iacono W. The status of spectral EEG abnormality as a diagnostic test for schizophrenia. Schizophr Res. 2008;99(1-3):225-237.

111. Benjamini Y, Hochberg Y. Controlling the False Discovery Rate - a Practical and Powerful Approach to Multiple Testing. J R Stat Soc B. 1995;57(1):289-300.

112. Zakar-Polyák E, Nagy M, Molontay R. Towards a better understanding of the characteristics of fractal networks. Applied Network Science. 2023;8(1):17.

113. Yeo BTT, Krienen FM, Sepulcre J, Sabuncu MR, Lashkari D, Hollinshead M, Roffman JL, Smoller JW, Zoller L, Polimeni JR, Fischl B, Liu HS, Buckner RL. The organization of the human cerebral cortex estimated by intrinsic functional connectivity. J Neurophysiol. 2011;106(3):1125-1165.

114. Giacometti P, Perdue KL, Diamond SG. Algorithm to find high density EEG scalp coordinates and analysis of their correspondence to structural and functional regions of the brain. J Neurosci Methods. 2014;229:84-96.

115. Klimesch W, Doppelmayr M, Schimke H, Ripper B. Theta synchronization and alpha desynchronization in a memory task. Psychophysiology. 1997;34(2):169-176.

116. Wink AM, Bullmore E, Barnes A, Bernard F, Suckling J. Monofractal and multifractal dynamics of low frequency endogenous brain oscillations in functional MRI. Hum Brain Mapp. 2008;29(7):791-801.

117. Kaposzta Z, Czoch A, Mukli P, Stylianou O, Liu DH, Eke A, Racz FS. Fingerprints of decreased cognitive performance on fractal connectivity dynamics in healthy aging. GeroScience. 2024;46(1):713-736.

118. Rabbitt P, Lowe C. Patterns of cognitive ageing. Psychol Res-Psych Fo. 2000;63(3-4):308-316.

119. Wild K, Howieson D, Webbe F, Seelye A, Kaye J. Status of computerized cognitive testing in aging: A systematic review. Alzheimers & Dementia. 2008;4(6):428-437.

120. Csipo T, Lipecz A, Fulop GA, Hand RA, Ngo BTN, Dzialendzik M, Tarantini S, Balasubramanian P, Kiss T, Yabluchanska V, Silva-Palacios F, Courtney DL, Dasari TW, Sorond F, Sonntag WE, Csiszar A, Ungvari Z, Yabluchanskiy A. Age-related decline in peripheral vascular health predicts cognitive impairment. Geroscience. 2019;41(2):125-136.

121. Endrass T, Schreiber M, Kathmann N. Speeding up older adults: Age-effects on error processing in speed and accuracy conditions. Biol Psychol. 2012;89(2):426-432.

122. Starns JJ, Ratcliff R. The Effects of Aging on the Speed-Accuracy Compromise: Boundary Optimality in the Diffusion Model. Psychology and Aging. 2010;25(2):377-390.

123. Peich MC, Husain M, Bays PM. Age-Related Decline of Precision and Binding in Visual Working Memory. Psychology and Aging. 2013;28(3):729-743.

124. Carriere JSA, Cheyne JA, Solman GJF, Smilek D. Age Trends for Failures of Sustained Attention. Psychology and Aging. 2010;25(3):569-574.

125. Loveless NE, Sanford AJ. Effects of age on the contingent negative variation and preparatory set in a reaction-time task. J Gerontol. 1974;29(1):52-63.

126. Michalewski HJ, Thompson LW, Smith DB, Patterson JV, Bowman TE, Litzelman D, Brent G. Age differences in the contingent negative variation (CNV): reduced frontal activity in the elderly. J Gerontol. 1980;35(4):542-549.

127. Brustio PR, Magistro D, Zecca M, Rabaglietti E, Liubicich ME. Age-related decrements in dual-task performance: Comparison of different mobility and cognitive tasks. A cross sectional study. PLoS One. 2017;12(7):e0181698.

128. Andrews-Hanna JR, Snyder AZ, Vincent JL, Lustig C, Head D, Raichle ME, Buckner RL. Disruption of large-scale brain systems in advanced aging. Neuron. 2007;56(5):924-935.

129. Vecchio F, Miraglia F, Marra C, Quaranta D, Vita MG, Bramanti P, Rossini PM. Human brain networks in cognitive decline: a graph theoretical analysis of cortical connectivity from EEG data. J Alzheimers Dis. 2014;41(1):113-127.

130. Stumme J, Krämer C, Miller T, Schreiber J, Caspers S, Jockwitz C. Interrelating differences in structural and functional connectivity in the older adult's brain. Hum Brain Mapp. 2022;43(18):5543-5561.

131. Stylianou O, Kaposzta Z, Czoch A, Stefanovski L, Yabluchanskiy A, Racz FS, Ritter P, Eke A, Mukli P. Scale-Free Functional Brain Networks Exhibit Increased Connectivity, Are More Integrated and Less Segregated in Patients with Parkinson's Disease following Dopaminergic Treatment. Fractal Fract. 2022;6(12).

132. Buzsaki G. Rhythms of the Brain: Oxford University Press; 2006.

133. Bak P, Tang C, Wiesenfeld K. Self-organized criticality: An explanation of the 1/f noise. Physical review letters. 1987;59(4):381-384.

134. Chialvo DR. Critical brain networks. Physica A. 2004;340(4):756-765.

135. Hesse J, Gross T. Self-organized criticality as a fundamental property of neural systems. Front Syst Neurosci. 2014;8:166.

136. Beggs JM, Timme N. Being critical of criticality in the brain. Front Physiol. 2012;3:163.

137. Poil SS, Hardstone R, Mansvelder HD, Linkenkaer-Hansen K. Critical-state dynamics of avalanches and oscillations jointly emerge from balanced excitation/inhibition in neuronal networks. J Neurosci. 2012;32(29):9817-9823.

138. Schirner M, Mclntosh AR, Jirsa V, Deco G, Ritter P. Inferring multi-scale neural mechanisms with brain network modelling. Elife. 2018;7.

139. Doval S, Nebreda A, Bruña R. Functional connectivity across the lifespan: a cross-sectional analysis of changes. Cereb Cortex. 2024;34(10).

140. Agosta F, Sala S, Valsasina P, Meani A, Canu E, Magnani G, Cappa SF, Scola E, Quatto P, Horsfield MA, Falini A, Comi G, Filippi M. Brain network connectivity assessed using graph theory in frontotemporal dementia. Neurology. 2013;81(2):134-143.

141. Davis SW, Kragel JE, Madden DJ, Cabeza R. The architecture of cross-hemispheric communication in the aging brain: linking behavior to functional and structural connectivity. Cereb Cortex. 2012;22(1):232-242.

142. Owen AM, McMillan KM, Laird AR, Bullmore E. N-back working memory paradigm: a meta-analysis of normative functional neuroimaging studies. Hum Brain Mapp. 2005;25(1):46-59.

143. Nyberg L, Lovden M, Riklund K, Lindenberger U, Backman L. Memory aging and brain maintenance. Trends in cognitive sciences. 2012;16(5):292-305.

144. Pardo JV, Fox PT, Raichle ME. Localization of a Human System for Sustained Attention by Positron Emission Tomography. Nature. 1991;349(6304):61-64.

145. Kimberg DY, D'Esposito M, Farah MJ. Cognitive functions in the prefrontal cortex - Working memory and executive control. Curr Dir Psychol Sci. 1997;6(6):185-192.

146. Bennett PJ, Sekuler AB, McIntosh AR, Della-Maggiore V. The effects of aging on visual memory: evidence for functional reorganization of cortical networks. Acta Psychol. 2001;107(1-3):249-273.

147. Jauny G, Mijalkov M, Canal-Garcia A, Volpe G, Pereira J, Eustache F, Hinault T. Linking structural and functional changes during aging using multilayer brain network analysis. Commun Biol. 2024;7(1):239.

148. Ciuciu P, Varoquaux G, Abry P, Sadaghiani S, Kleinschmidt A. Scale-Free and Multifractal Time Dynamics of fMRI Signals during Rest and Task. Front Physiol. 2012;3:186.

149. Zilber N, Ciuciu P, Abry P, van Wassenhove V. Modulation of Scale-Free Properties of Brain Activity in Meg. 9th IEEE Isbi. 2012:1531-1534.

150. Huang ZR, Ohara N, Davis H, Pokorny J, Northoff G. The temporal structure of resting-state brain activity in the medial prefrontal cortex predicts self-consciousness. Neuropsychologia. 2016;82:161-170.

151. Kolvoort IR, Wainio-Theberge S, Wolff A, Northoff G. Temporal integration as "common currency" of brain and self-scale-free activity in resting-state EEG correlates with temporal delay effects on self-relatedness. Hum Brain Mapp. 2020.

152. Tolkunov D, Rubin D, Mujica-Parodi LR. Power spectrum scale invariance quantifies limbic dysregulation in trait anxious adults using fMRI: Adapting methods optimized for characterizing autonomic dysregulation to neural dynamic time series. Neuroimage. 2010;50(1):72-80.

153. Gao R, Peterson EJ, Voytek B. Inferring synaptic excitation/inhibition balance from field potentials. NeuroImage. 2017;158:70-78.

154. Ivanov P, Nunes Amaral LA, Goldberger AL, Stanley HE. Stochastic feedback and the regulation of biological rhythms. Europhys Lett. 1998;43(4):363-368.

155. Bak P. How nature works: the science of self-organized criticality. New York: Springer Science & Business Media; 1996.

156. Gisiger T. Scale invariance in biology: coincidence or footprint of a universal mechanism? Biol Rev. 2001;76(2):161-209.

157. Mitra PP, Pesaran B. Analysis of dynamic brain imaging data. Biophys J. 1999;76(2):691-708.

158. Nagy Z, Mukli P, Herman P, Eke A. Decomposing multifractal crossovers. Front Physiol. 2017;8(JUL):533.

159. Benzi R, Paladin G, Parisi G, Vulpiani A. On the Multifractal Nature of Fully-Developed Turbulence and Chaotic Systems. J Phys a-Math Gen. 1984;17(18):3521-3531.

160. Mandelbrot BB. Multifractals and Fractals. Phys Today. 1986;39(9):11.

161. Ivanov PC, Amaral LA, Goldberger AL, Havlin S, Rosenblum MG, Struzik ZR, Stanley HE. Multifractality in human heartbeat dynamics. Nature. 1999;399(6735):461-465.

162. Shimizu Y, Barth M, Windischberger C, Moser E, Thurner S. Wavelet-based multifractal analysis of fMRI time series. Neuroimage. 2004;22(3):1195-1202.

163. Podobnik B, Horvatic D, Petersen AM, Stanley HE. Cross-correlations between volume change and price change. PNAS. 2009;106(52):22079-22084.

164. Kaposzta Z, Czoch A, Stylianou O, Kim K, Mukli P, Eke A, Racz FS. Real-Time Algorithm for Detrended Cross-Correlation Analysis of Long-Range Coupled Processes. Front Physiol. 2022;13.

9 Bibliography of the candidate's publications

9.1 Publications forming the basis of the thesis

- **Czoch, Akos**, Zalan Kaposzta, Peter Mukli, Orestis Stylianou, Andras Eke, and Frigyes Samuel Racz. "**Resting-state fractal brain connectivity is associated with impaired cognitive performance in healthy aging**." GeroScience 46, no. 1 (2024): 473-489.
    - Impact factor: 5,4 (2025)
- Racz, Frigyes Samuel, **Akos Czoch**, Zalan Kaposzta, Orestis Stylianou, Peter Mukli, and Andras Eke. "**Multiple-resampling cross-spectral analysis: an unbiased tool for estimating fractal connectivity with an application to neurophysiological signals.**" Frontiers in Physiology 13 (2022): 817239
    - Impact factor: 4,0 (2025)

9.2 Additional publications from the candidate

Racz FS, Farkas K, Stylianou O, Kaposzta Z, Czoch A, Mukli P, Csukly G, Eke A. Separating scale-free and oscillatory components of neural activity in schizophrenia. Brain Behav. 2021;11(5):e02047.

Stylianou O, Kaposzta Z, Czoch A, Stefanovski L, Yabluchanskiy A, Racz FS, Ritter P, Eke A, Mukli P. Scale-Free Functional Brain Networks Exhibit Increased Connectivity, Are More Integrated and Less Segregated in Patients with Parkinson's Disease following Dopaminergic Treatment. Fractal Fract. 2022;6(12).

Kaposzta Z, Czoch A, Stylianou O, Kim K, Mukli P, Eke A, Racz FS. Real-Time Algorithm for Detrended Cross-Correlation Analysis of Long-Range Coupled Processes. Front Physiol. 2022;13.

Stylianou O, Racz FS, Kim K, Kaposzta Z, Czoch A, Yabluchanskiy A, Eke A, Mukli P. Multifractal Functional Connectivity Analysis of Electroencephalogram Reveals Reorganization of Brain Networks in a Visual Pattern Recognition Paradigm. Front Hum Neurosci. 2021;15:740225.

Kaposzta Z, Czoch A, Mukli P, Stylianou O, Liu DH, Eke A, Racz FS. Fingerprints of decreased cognitive performance on fractal connectivity dynamics in healthy aging. GeroScience. 2024;46(1):713-736.

Racz FS, Kumar S, Kaposzta Z, Alawieh H, Liu DH, Liu R, Czoch A, Mukli P, Millán JdR. Combining detrended cross-correlation analysis with Riemannian geometry-based classification for improved brain-computer interface performance. Front Neurosci. 2024;Volume 18 - 2024.

10 Acknowledgements

I would like to express my gratitude to my supervisor Frigyes Sámuel Rácz for the continuous support, the complete trust in my work, the straightforward conversations and for guiding me through this endeavour. I also deeply thank Prof. Attila Mócsai, the head of Department of Physiology, for supporting my PhD work in the department. My sincere thanks go to our lab, Dr. András Eke, Dr. Péter Mukli, Dr. Orestis Stylianou and Dr. Zalán Balázs Káposzta for the support, help, good advice and company. My deepest gratitude goes to Dr. Eszter Horváth, who supported, advised and helped me in any way imaginable. I would like to thank the support of all colleagues from the Department of Physiology. I also would like to thank our participants. This dissertation could not have been completed without their contribution. I am profoundly thankful to my Friends, who did not choose to embark on this adventure, yet they stuck with me through it all. Last, but not least, I am grateful for my Family for their continuous and unconditional love and support. I am sure that I would not have been able to finish my PhD without them.